AD-A103 110 SRI INTERNATIONAL MENLO PARK CA F/G 4/1
RADAR OBSERVATIONS OF STRUCTURED PLASMA IN THE HIGH-LATITUDE F --ETC(U)
MAR 81 J F VICKREY DNA001-80-C-0015
UNCLASSIFIED DNA-5648F NL

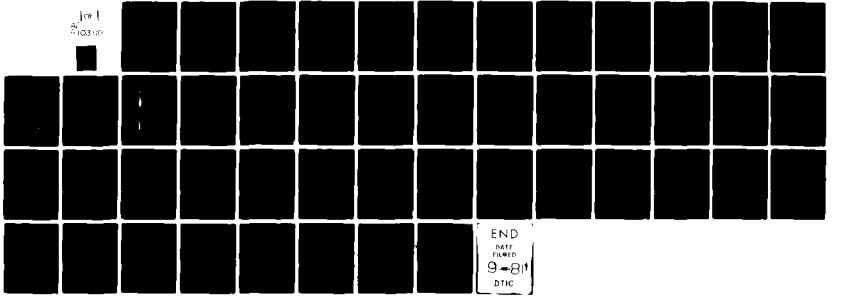

END
DATE FILMED
9-81
DTIC

DNA 5645F

RADAR OBSERVATIONS OF STRUCTURED PLASMA IN THE HIGH-LATITUDE F REGION

James F. Vickrey
SRI International
333 Ravenswood Avenue
Menlo Park, California 94025

31 Mar 81

Final Report 14 Jan 80—31 Mar 81

CONTRACT No. DNA 001-80-C-0015

THIS WORK SPONSORED BY THE DEFENSE NUCLEAR AGENCY
UNDER RDT&E RMSS CODE B322080462 I25AAXHX64015 H2590D.

Prepared for
Director
DEFENSE NUCLEAR AGENCY
Washington, D. C. 20305

Destroy this report when it is no longer needed. Do not return to sender.

PLEASE NOTIFY THE DEFENSE NUCLEAR AGENCY, ATTN: STTI, WASHINGTON, D.C. 20305, IF YOUR ADDRESS IS INCORRECT, IF YOU WISH TO BE DELETED FROM THE DISTRIBUTION LIST, OR IF THE ADDRESSEE IS NO LONGER EMPLOYED BY YOUR ORGANIZATION.

UNCLASSIFIED

SECURITY CLASSIFICATION OF THIS PAGE (When Data Entered)

REPORT DOCUMENTATION PAGE		READ INSTRUCTIONS BEFORE COMPLETING FORM
1. REPORT NUMBER DNA 5645F	2. GOVT ACCESSION NO.	3. RECIPIENT'S CATALOG NUMBER
4. TITLE (and Subtitle) RADAR OBSERVATIONS OF STRUCTURED PLASMA IN THE HIGH-LATITUDE F REGION		5. TYPE OF REPORT & PERIOD COVERED Final Report for Period 14 Jan 80-31 Mar 81
		6. PERFORMING ORG. REPORT NUMBER SRI Project 1276
7. AUTHOR(s) James F. Vickrey		8. CONTRACT OR GRANT NUMBER(s) DNA 001-80-C-0015
9. PERFORMING ORGANIZATION NAME AND ADDRESS SRI International 333 Ravenswood Avenue Menlo Park, California 94025		10. PROGRAM ELEMENT, PROJECT, TASK AREA & WORK UNIT NUMBERS Subtask I25AAXHX640-15
11. CONTROLLING OFFICE NAME AND ADDRESS Director Defense Nuclear Agency Washington, D.C. 20305		12. REPORT DATE 31 March 1981
		13. NUMBER OF PAGES 48
14. MONITORING AGENCY NAME & ADDRESS(if different from Controlling Office)		15. SECURITY CLASS (of this report) UNCLASSIFIED
		15a. DECLASSIFICATION/DOWNGRADING SCHEDULE

16. DISTRIBUTION STATEMENT (of this Report)

Approved for public release; distribution unlimited

17. DISTRIBUTION STATEMENT (of the abstract entered in Block 20, if different from Report)

18. SUPPLEMENTARY NOTES

This work sponsored by the Defense Nuclear Agency under RDT&E RMSS Code B322080462 I25AAXHX64015 H2590D.

19. KEY WORDS (Continue on reverse side if necessary and identify by block number)

Structured plasma
Irregularities
Current convective instability
Gradient drift
Instability
Scintillation
Plasma blobs

20. ABSTRACT (Continue on reverse side if necessary and identify by block number)

Results are presented from a campaign of coordinated measurements between the Chatanika radar and the TRIAD satellite to investigate the production mechanisms responsible for localized high-latitude scintillation. The radar measured the latitudinal variations of plasma density and electric field while the satellite measured the latitudinal variation of field-aligned current. This information was used to assess the stability of the observed plasma configuration. Field-aligned ionization enhancements or plasma "blobs" with

DD FORM 1 JAN 73 1473 EDITION OF 1 NOV 65 IS OBSOLETE

UNCLASSIFIED

SECURITY CLASSIFICATION OF THIS PAGE (When Data Entered)

steep poleward and equatorward edges were found to be a common feature of the midnight-sector auroral F region. Their presence is not strongly related to magnetic activity nor to E-region processes. The plasma blobs are unstable to the current convective instability with growth rates of several millihertz. They are unstable to the gradient drift instability on either the poleward or equatorward edge, depending on the electric field and neutral-wind configuration. Field-aligned currents have a further destabilizing influence, but seldom (if ever) dominate the electric-field contribution to instability. The presence of plasma density irregularities associated with the blobs was verified by observing scintillation on the TRIAD satellite telemetry signal at 150 MHz. The F-region irregularities exist despite the presence of a highly conducting auroral E region to which the F-region plasma is connected by the geomagnetic field lines. The F-region blobs and their associated irregularities convect with the background electric field. Because large scale ($\sim$ 1) irregularities can have long lifetimes, they may exist far from where they were originally produced.

TABLE OF CONTENTS

SECTION		PAGE
	LIST OF ILLUSTRATIONS	2
I	INTRODUCTION.	3
II	F-REGION IRREGULARITY PRODUCTION MECHANISMS	6
III	COLLOCATION OF SCINTILLATION PATCHES AND F-REGION IONIZATION ENHANCEMENTS.	7
IV	STABILITY OF F-REGION IONIZATION ENHANCEMENTS	15
V	E-REGION CONDUCTIVITY CONSIDERATIONS	19
VI	ON THE ORIGIN AND THERMAL STRUCTURE OF AURORAL F-REGION IONIZATION ENHANCEMENTS.	21
VII	IRREGULARITY LIFETIME CONSIDERATIONS AND IMPLICATIONS FOR GLOBAL SCINTILLATION MORPHOLOGY. . . .	33
VIII	SUMMARY	37
	REFERENCES	38

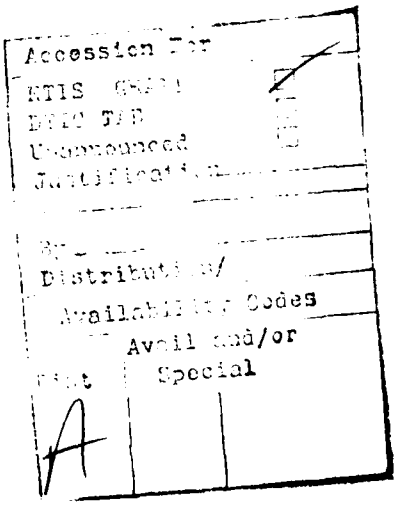

LIST OF ILLUSTRATIONS

Figure		Page
1	Altitude/Latitude Variation of Electron Density--27 February 1980, 0932 to 0945 UT	8
2	Altitude/Latitude Variation of Electron Density--27 February 1980, 0945 to 0958 UT	9
3	Latitudinal Variation of Intensity Scintillation and the S_4 Index	11
4	Geometry of TRIAD Trajectory and the Radar Scan--27 February 1980, 9:47 to 0958 UT	12
5	TRIAD Magnetometer Data (Geomagnetic Frame)	14
6	Latitudinal Variation of Electric Field, Field-Aligned Current, and the Maximum Growth Rate of the Current Convective Instability--27 February 1980, 0945 to 0957 UT	17
7	Altitude/Latitude Variation of Electron Density--27 February 1980, 0945 to 0958 UT	23
8	Latitudinal Variation of Electron and Ion Temperature and Electron Density at Two Fixed Altitudes	24
9	Measured Values of Electron and Ion Temperature as an Enhanced F_2 Layer Passed Through the Beam	26
10	Altitude/Latitude Variation of Electron Density--23 February 1980, 111538 to 112810 UT	27
11	Altitude/Latitude Variation of Electron Density--23 February 1980, 112811 to 114043 UT	28
12	Altitude/Latitude Variation of Electron Density--23 February 1980, 114043 to 115316 UT	29
13	Altitude/Latitude Variation of Electron Density--23 February 1980, 115316 to 120549 UT	30
14	Altitude/Latitude Variation of Electron Density--1 March 1980, 094948 to 100221 UT	34

I INTRODUCTION

Plasma-density irregularities are present virtually throughout the F-region ionosphere of the auroral zone and polar cap. The plasma is structured on a spatial scale that ranges from tens of kilometers to tens of meters. These irregularities cause scintillation of radio waves that cross the disturbed region. The most comprehensive study of high-latitude scintillations carried out to date made use of the large body of data collected from the Wideband satellite (Rino et al., 1980, and references therein). Statistically, the most prominent feature of the Wideband auroral-zone data is a localized scintillation enhancement that occurs at the latitude at which the propagation vector lies within the local L shell. The unique location of the enhancement leads to the hypothesis that the geometry of the irregularities has L-shell-aligned sheet-like anisotropy. This interpretation is supported by spaced-receiver interferometer measurements performed by Rino et al. (1978). Rino and Matthews (1979) showed, however, that these scintillation enhancements cannot be explained purely in terms of a geometric enhancement alone. They noted that the enhancements disappear when magnetic activity is very low ($K \sim 0$) even though significant scintillation levels are present where the geometric enhancement should occur. This suggests that a dynamic source region may be responsible for the irregularities.

By comparing simultaneous scintillation measurements at two latitudes along the magnetic meridian, Rino and Owen (1980) showed that the source regions where the sheet-like structures develop are confined in latitude. Indeed, they proposed that the source region is a vertical "slab" of F-region plasma. By carefully comparing the latitudinal variations in total electron content measured at the two stations, they inferred a steep electron-density gradient at the equatorward edge of the slab. The presence of this steep horizontal density gradient suggests that a plasma instability may be the source mechanism. However, because their

measurements were from the midnight sector, where the zonal electric-field component is typically westward, the steep poleward gradient at the equatorward edge of the slab is stable to the gradient drift instability. This stability led Ossakow and Chaturvedi (1979) to propose the current convective instability as the source mechanism because moderately intense field-aligned currents (which are known to flow in the auroral zone) can destabilize an otherwise stable plasma configuration.

This report documents the results of a campaign of coordinated measurements between the Chatanika radar and the TRIAD satellite to investigate the production mechanisms responsible for localized high-latitude scintillations. The radar measured the latitudinal variations of plasma density and electric field while the satellite measured the field-aligned current distribution with latitude. This information was used to assess the stability of the plasma configuration.

Unstable field-aligned ionization enhancements (or plasma "blobs") are a very common feature of the midnight-sector auroral zone. Moreover, both the equatorward and poleward edges of the blobs can be very steep. Therefore, depending on the sign of the zonal electric-field component, either one side of the blob or the other will be gradient drift unstable even without a field-aligned current. On that side, the field-aligned current if present, further destabilizes an already unstable plasma configuration. In principle, the $\underline{E} \times \underline{B}$ stable side of the blob can be destabilized by a field-aligned current if the current is sufficiently intense to overcome the stabilizing effects of $\underline{E}$. However, at the latitudes and local times of the measurements presented, the field-aligned currents that were observed were too weak for this to occur. In fact, even on the $\underline{E} \times \underline{B}$ unstable side, their contribution to the linear growth rate of the current convective instability was generally ≤ 10 percent. However, this situation may be very different at other locations, such as the polar cusp where the field-aligned currents are more intense. Furthermore, even weak currents, if structured in latitude, can contribute to the formation and edge steepening of plasma blobs (see Section VI).

The thermal structure of the observed blobs suggests that most are not locally produced, but convect into the radar field of view with the

background electric field. The large-scale irregularities (≥ 1 km) produced in the unstable regions have lifetimes on the order of hours. Therefore, convection probably plays an important role in defining the global morphology of high-latitude scintillation. Furthermore, there is no reason to expect scintillation boundaries to correlate on a one-to-one basis with precipitation boundaries. At present, convection effects are not accounted for in global scintillation models such as that used by Air Weather Service. These effects are described in detail in Section VII of this report.

Finally, it is important to emphasize the complimentary character of the high-latitude and equatorial irregularity-formation mechanisms. The linear instabilities operating in the F region at the equator are analogous to those discussed here after allowances are made for proper geometry changes. A critical difference, however, is that the F-region plasma at high latitudes can be connected directly to a highly conducting, precipitation-produced, E region in the auroral zone whereas the nighttime equatorial E region is essentially an open circuit. Thus, the present observations provide an opportunity to test numerical simulations of F-region instabilities with an entirely different set of boundary conditions.

II F-REGION IRREGULARITY PRODUCTION MECHANISMS

The characteristics of, and the physical mechanisms responsible for, high-latitude electron density irregularities in general have been reviewed by Fejer and Kelley (1980). Irregularities can result from structured particle precipitation, electrostatic turbulence, or plasma instability. In the situation here, however, plasma instability seems to be the most likely candidate. The gradient drift instability, for example, can result in scintillation-producing irregularities because virtually all scale sizes are unstable; it is wavelength-dependent damping that favors growth at some scale sizes. The linear gradient drift and current convective instabilities, however, favor growth of spatial-wave vectors normal to the electron density gradient, which is meridional in the auroral case. Because the scintillation data from the WIDEBAND satellite indicate that the irregularities are L-shell aligned, it is clear that the linear instabilities alone cannot explain the observations. Chaturvedi and Ossakow (1979a,b) have resolved this apparent paradox by their analysis, which shows that the linearly unstable mode of the gradient drift and current convective instabilities can transfer energy through nonlinear coupling to a mode whose wave vector lies in the plane of the density gradient.

To examine directly the role of instabilities in structuring F-region plasma, an experiment was performed at Chatanika, Alaska, that combined simultaneous measurements of (1) the latitudinal distribution of plasma density and electric fields using the Chatanika radar and (2) in-situ measurements of the latitudinal distribution of field-aligned currents from the TRIAD satellite, which passed nearly directly over Chatanika in the midnight sector. This information, combined with a model collision frequency profile, was used to calculate the linear growth rate of the current convective instability. The regions of enhanced scintillation are associated with F-region ionization enhancements that are linearly unstable.

III COLLOCATION OF SCINTILLATION PATCHES AND F-REGION IONIZATION ENHANCEMENTS

During late February and early March 1980, the TRIAD satellite passed nearly directly over the Chatanika radar during the midnight sector. To take advantage of the favorable geometry for comparing simultaneous measurements from TRIAD and the Chatanika radar, a campaign of measurements was conducted during seven nights. For several hours each night the Chatanika radar continuously scanned the magnetic meridional plane before, during, and after each satellite pass. When operated in this mode, the radar can map the altitude/latitude distribution of electron density and bulk plasma motion (electric fields) over the altitude range from 85 to 500 km, and the invariant latitude range from 64° to 67° in about 12 minutes (Vondrak and Baron, 1976). Transmitter pulses 60 μs and 320 μs long were used to provide 9-km and 48-km resolution for the electron-density measurements and good signal-to-noise ratio for the velocity measurements. The data were integrated for 15 s, giving $\sim$ 3° angular resolution in the meridional plane.

Figure 1 shows the altitude/latitude distribution of electron density measured between 0932 and 0945 UT* on 27 February 1980. In constructing this map, the measured line-of-sight electron-density profiles have been transformed into a coordinate system that has straight, vertical magnetic field lines. The presence of two F-region ionization enhancements (labeled 1 and 2) with large meridional density gradients perpendicular to the magnetic field is striking.

Figure 2 shows a similar map of constant electron-density contours measured on the next meridian scan. During this scan from north to south, the radar beam led the TRIAD satellite position by $\sim$1 minute.

*Local time is UT minus 10 hours.

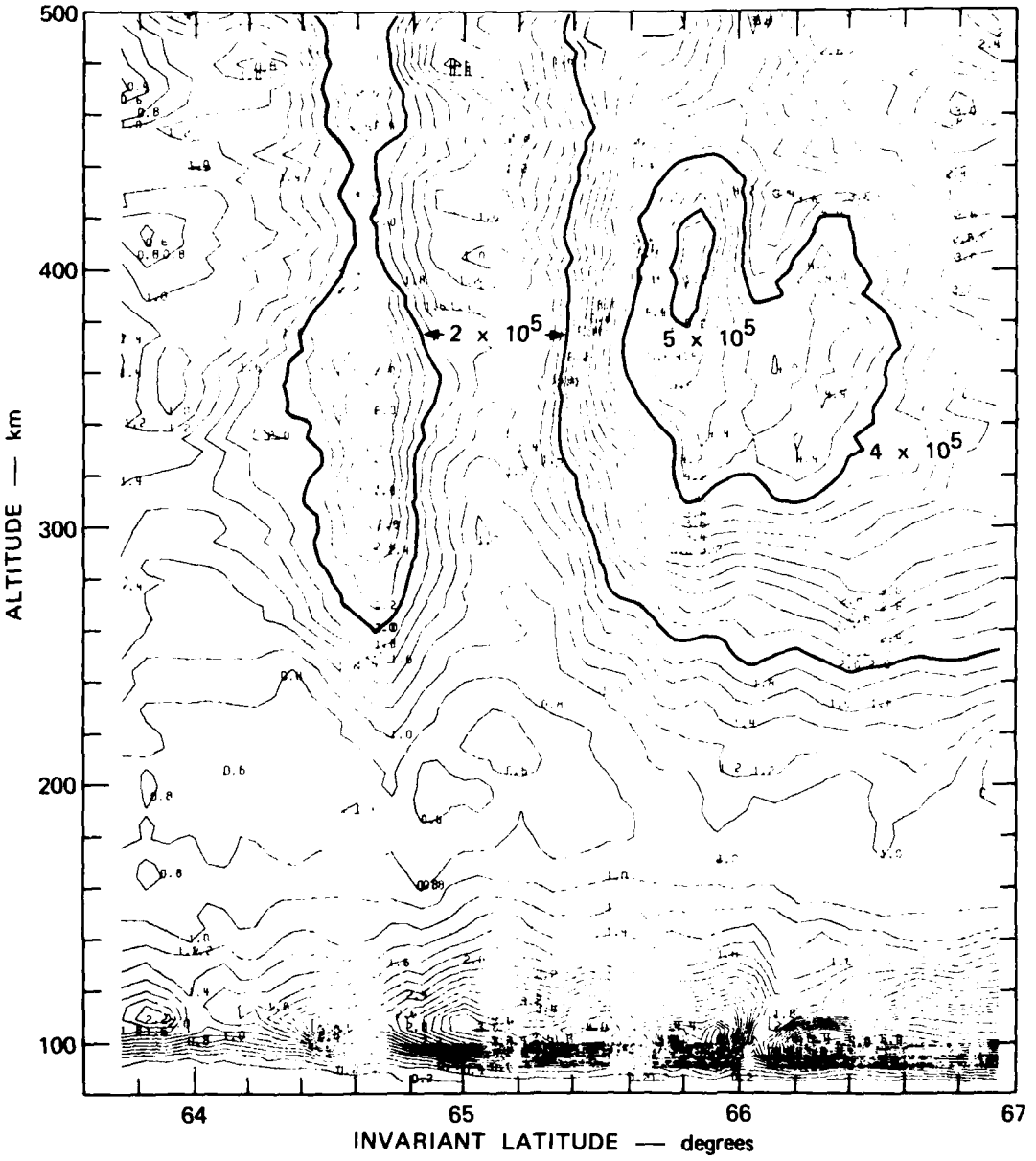

FIGURE 1 ALTITUDE/LATITUDE VARIATION OF ELECTRON DENSITY — 27 FEBRUARY 1980, 0932 TO 0945 UT

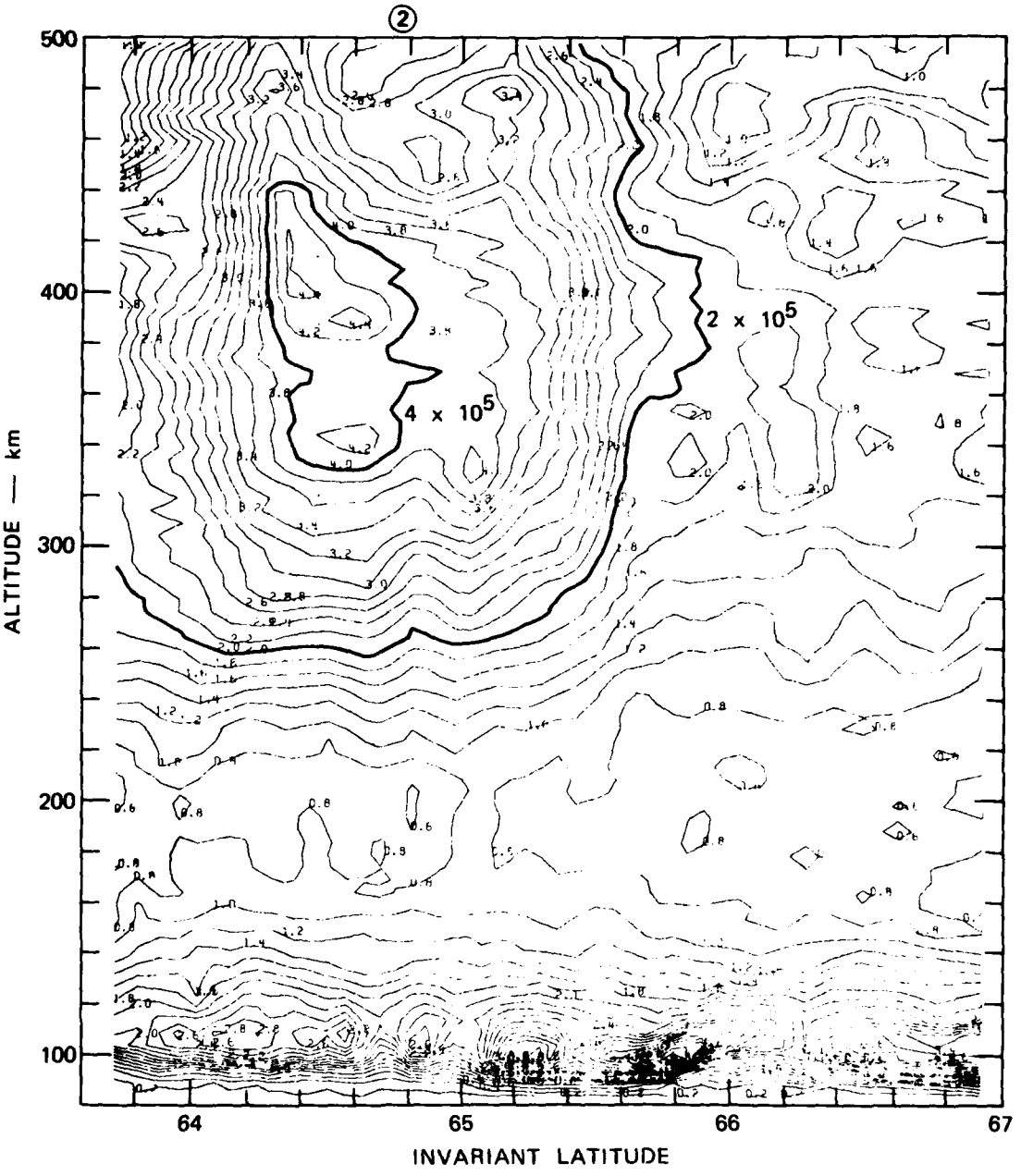

FIGURE 2 ALTITUDE/LATITUDE VARIATION OF ELECTRON DENSITY — 27 FEBRUARY 1980, 0945 TO 0958 UT

Both enhancements moved south by $\sim 1.4°$ of latitude, which is consistent with the measured westward electric field component. Enhancement 1 has moved south of the field of view shown in this figure, but was located at $\sim 63.2°$ invariant latitude. As shown below, enhanced scintillation on the TRIAD telemetry signal was associated with both F-region features.

Figure 3 shows the severe amplitude fading of the TRIAD 150-MHz telemetry signal as it passed from north to south over Chatanika. At closest approach, the elevation angle of the satellite was 82°. Also indicated in Figure 3 is the measured value of the scintillation index S_4($S_4^2 = (\langle I^2 \rangle - \langle I \rangle^2) / \langle I^2 \rangle$, I = intensity). The observed enhancements in the S_4 index can be separated into three distinct latitude regimes. North of Chatanika is a latitudinally broad region of enhanced scintillation (labeled A), whose magnitude increases with increasing latitude. Overhead and to the south are two distinct scintillation "patches," labeled B and C. The dashed curve is a model calculation of the expected geometric enhancement in scintillation for 10:10:1 sheet-like irregularities (Rino, 1979).

To associate the scintillation patches with the enhanced F-region electron-density structures, the geographical location of the penetration point of the satellite signal at 350-km altitude is plotted in Figure 4. The locations of the enhanced scintillation patches (for 350-km reference altitude) are labeled B and C. The F-region ionization enhancements that were measured in the magnetic meridional plane by the radar are labeled 1 and 2 . Note that the scintillation enhancements occur at essentially the same geomagnetic latitudes as the F-region ionization enhancements.

As discussed in the next section, analysis of the F-region ionization enhancements for the conditions appropriate to the current convective instability requires knowledge of the field-aligned current density, $J_\parallel$, flowing through the plasma. Fortunately, in-situ measurements of $J_\parallel$ are available for the present observations from the vector magnetometer aboard the TRIAD satellite. The magnetic perturbations measured by TRIAD

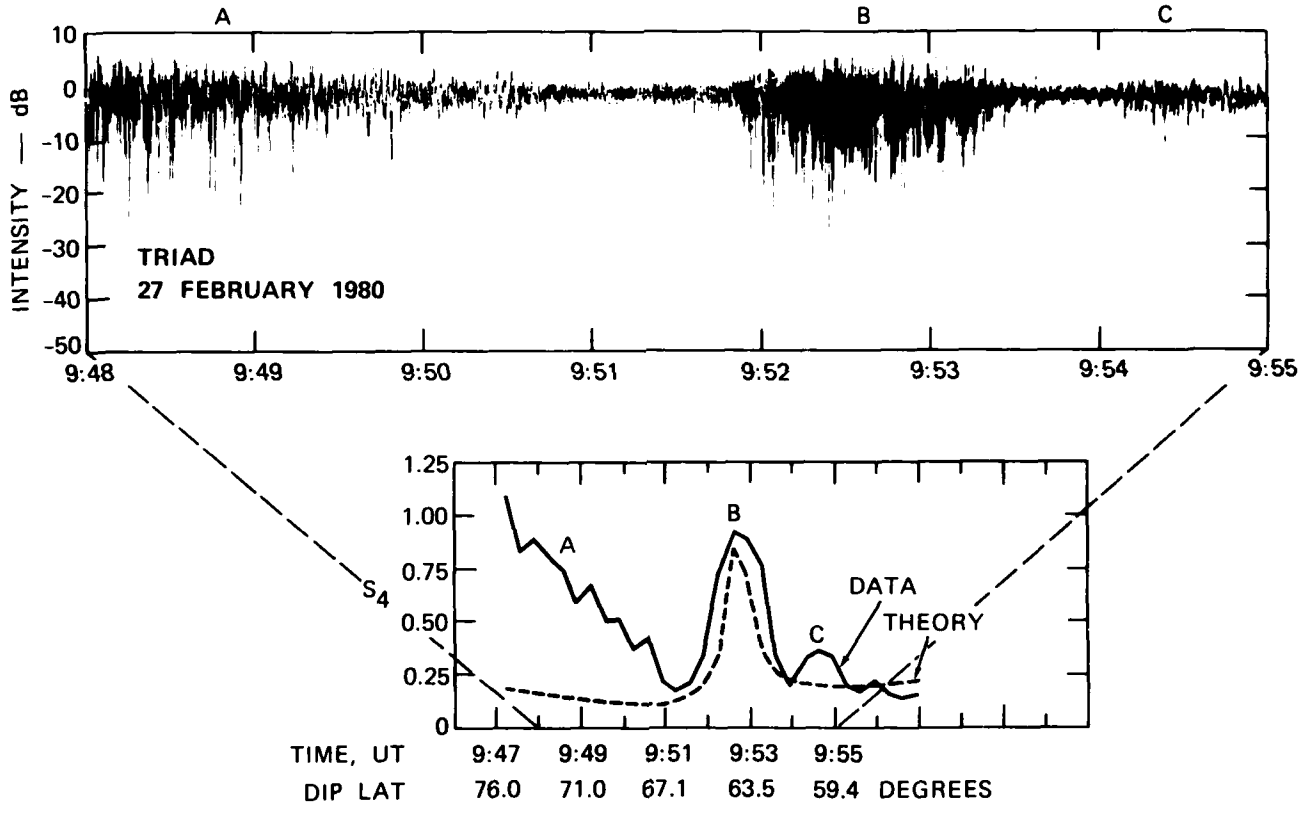

FIGURE 3 LATITUDINAL VARIATION OF INTENSITY SCINTILLATION AND THE S_4 INDEX

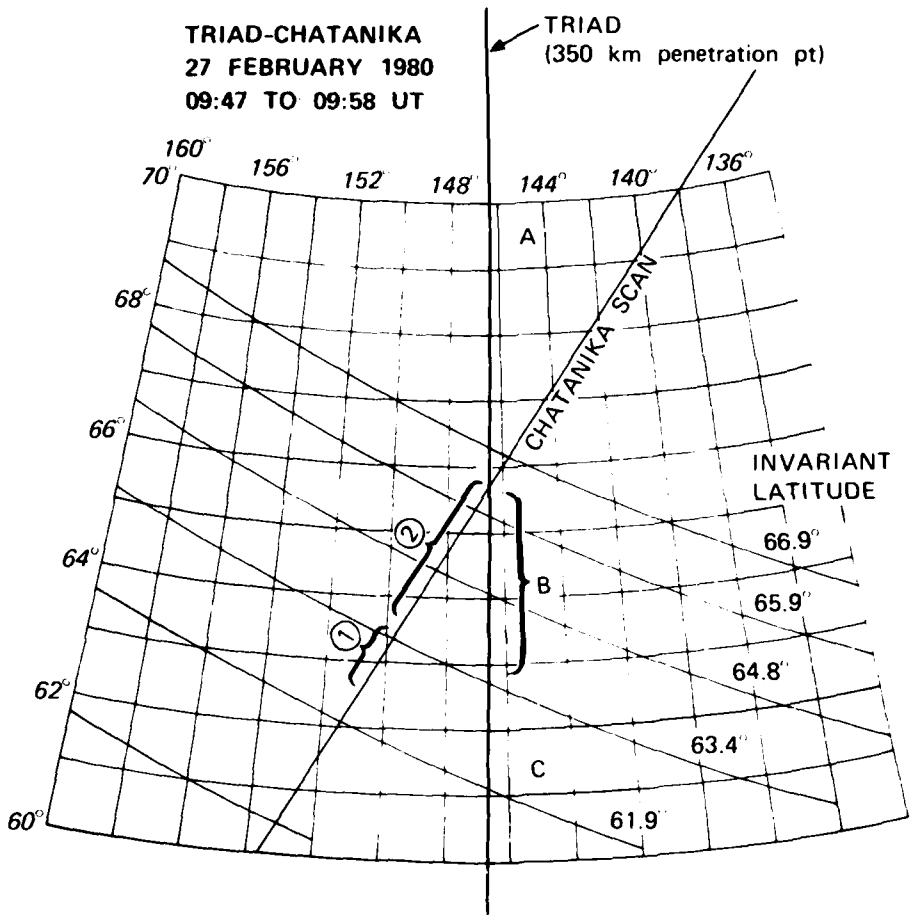

FIGURE 4 GEOMETRY OF TRIAD TRAJECTORY AND THE RADAR SCAN — 27 FEBRUARY 1980, 0947 TO 0958 UT

were transformed into geomagnetic north-south (B_θ) and east-west (B_θ) components in the manner described by Saflekos and Potemra (1980). The results are displayed in Figure 5. The large-scale variations in B_ϕ show a latitudinal behavior that is typical of the Harang discontinuity region (Iijima and Potemra, 1978)--namely, two regions of downward field-aligned current at high and low latitudes are separated by a region of upward field-aligned current. The latitudinal coverage obtained by the Chatanika radar scan is indicated on the figure. At the northernmost latitudes of radar coverage, the field-aligned current is small and upward. However, over the majority of the scan coverage, $J_\parallel$ is downward with a magnitude of $\sim 0.8\ \mu A/m^2$. Note the gap in TRIAD data at the southernmost portion of the radar field of view. This signal loss resulted from the strong scintillation associated with the F-region feature labeled 2 in Figure 2. Further, it is interesting that our estimate of the location of F-region slab 1 is coincident with a region of small-scale ($\leq$ 100 km) fluctuations in $\underline{B}$. Detailed analysis of such small-scale features is beyond the scope of this report and will be discussed elsewhere.

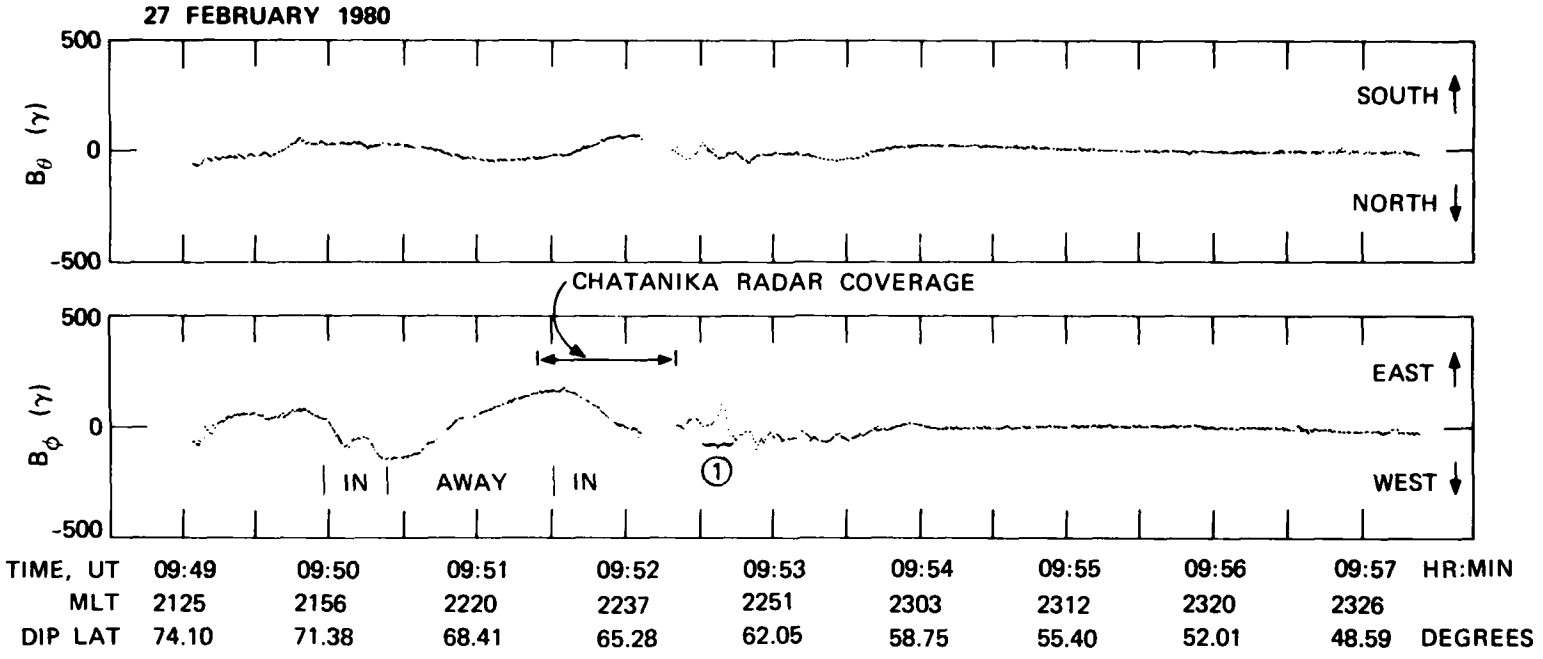

FIGURE 5 TRIAD MAGNETOMETER DATA (GEOMAGNETIC FRAME)

IV STABILITY OF F-REGION IONIZATION ENHANCEMENTS

As described above, the WIDEBAND satellite data indicate that, if the gradient drift or current convective instabilities are responsible for enhanced scintillation, they must already be in the nonlinear regime. Nevertheless, it is useful to calculate the linear growth rate of these instabilities to establish that the first order conditions for instability are met in the F-region ionization enhancements. Therefore, to assess the stability of the measured F-region plasma configurations, the maximum linear growth rate, γ_{max}, of the current convective instability [Ossakow and Chaturvedi, 1979; Chaturvedi and Ossakow, 1979b] has been calculated at each altitude and latitude surveyed by the radar.

$$\gamma_{max} = \frac{-\frac{1}{L}\left\{\frac{-E_x}{B}\frac{\nu_{in}}{\Omega_{in}} + V_d\,\theta_{max}\right\}}{\left[\frac{\Omega_i}{\nu_{in}} + \frac{\Omega_e}{\nu_{ei}}\right]\theta^2_{max} + \frac{\nu_{in}}{\Omega_i}} - k_\perp^2 \frac{\nu_{ei}}{\Omega_e\Omega_i} C_s^2 - \frac{k_\parallel^2 C_s^2}{\nu_{in}} \left\{1 + \frac{\nu_{in}^2/\Omega_i^2}{\frac{\nu_{ei}\nu_{in}}{\Omega_e\Omega_i} + \theta^2_{max}}\right\} \quad (1)$$

where $L^{-1} = \frac{1}{N}\frac{\partial N}{\partial y}$: N = electron density; y = a coordinate northward in the meridional plane and perpendicular to the magnetic field, $\underline{B}$; $V_d = J_\parallel/Nq$; $J_\parallel$ is parallel current (A/m^2); q = the electron change; and C_s = the ion-acoustic speed; ν_{in} and ν_{ei} = the ion-neutral and electron-ion collision frequencies; $\Omega_{e,i}$ = the electron and ion gyrofrequencies; and E_x = the eastward electric field. The ratio of parallel-to-perpendicular (to $\underline{B}$) wave numbers for maximum growth, θ_{max} [Ossakow and Chaturvedi, 1979] is given by:

$$\theta_{max} = \left(\frac{E_x}{BV_d}\right)\left(\frac{\nu_{in}}{\Omega_i}\right) \pm \left\{\left(\frac{E_x}{BV_d}\right)^2\left(\frac{\nu_{in}}{\Omega_i}\right)^2 + \frac{(\nu_{in}/\Omega_i)}{\left[\frac{\Omega_i}{\nu_{in}} + \frac{\Omega_e}{\nu_{ei}}\right]}\right\}^{1/2} . \quad (2)$$

Ion neutral collision frequencies were calculated using the coefficients of Schunk and Walker (1973), and the Jaccia 1972 neutral atmosphere model with exospheric temperature of 1000 K. The electron and ion temperatures were assumed equal to the model neutral temperature. The electron-ion collision frequency was estimated from $\nu_{ei} = 54\ N\ T_e^{-3/2}$ (Banks and Kockarts, 1973).

Note that if $k_{\parallel} \equiv 0$, Eq. (1) reduces to the growth rate of the gradient drift instability. Thus, a field-aligned current can serve to destabilize a plasma configuration that is otherwise stable to the gradient drift instability, or to enhance the growth rate of an already unstable situation.

The latitudinal variations in γ_{max} from Eq. (1) are plotted in Figure 6 at three altitudes for the radar scan corresponding to Figure 2. We have fixed $k_{\perp} = (2\pi/1000)m^{-1}$, and calculated the corresponding $k_{\parallel}$ according to Eq. (2). The choice of 1000 m for the perpendicular irregularity wavelength was made because 1000 m is close to the Fresnel dimension for the 150-MHz TRIAD signal. Also plotted in Figure 6 are the latitudinal variations in electric field and $J_{\parallel}$ as measured by TRIAD. The effect of magnetic flux tube divergence with height slightly increases the value of $J_{\parallel}$ with decreasing altitude. At the southernmost latitudes, where E_{west} is small, the F-region is only marginally stable. However, the F-region meridional neutral wind, which was not measured in this experiment, is normally southward in the midnight sector. Thus, our estimates for growth rate are too conservative in regions of northward density gradient. Furthermore, because the TRIAD signal was lost at these southermost latitudes, we have assumed $J_{\parallel}$ in this region is the same as the weak downward current measured farther north. If, instead, the current is intense and highly structured in this region as it is farther south, the plasma should be unstable. At 350- and 450-km altitude, γ_{max} becomes increasingly negative with latitude as the westward electric field increases. At $\sim 64.3°$ invariant latitude, γ_{max} becomes positive at 450 km because of the change in direction of $\nabla_{\perp}N$. By far, however, the largest growth rates at all F-region heights are measured on the poleward side of the electron-density enhancement where growth of

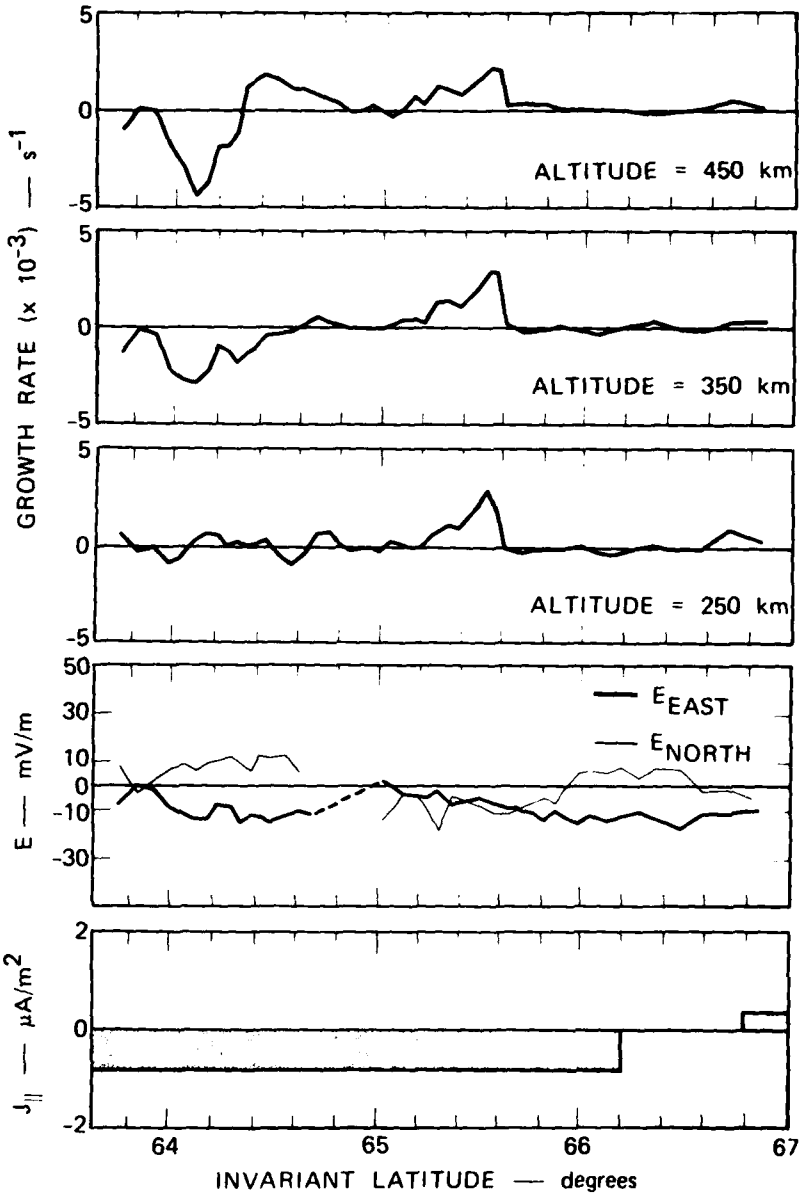

FIGURE 6 LATITUDINAL VARIATION OF ELECTRIC FIELD, FIELD-ALIGNED CURRENT, AND THE MAXIMUM GROWTH RATE OF THE CURRENT CONVECTIVE INSTABILITY — 27 FEBRUARY 1980, 0945 TO 0957 UT

the gradient-drift instability is enhanced by the presence of a field-aligned current.

Note that because the angular resolution of the radar scans in the meridional plane is $\sim 3°$ due to the 15-s data integration, very steep meridional density gradients may not have been resolved in our measurements. For example, at 350-km altitude, gradient scale lengths less than 35 km would not be resolved. In such cases the growth rates shown in Figure 6 should be increased.

V E-REGION CONDUCTIVITY CONSIDERATIONS

Note that the F-region irregularities detected in the experiment just discussed exist in an ambient background where the E-region Pedersen conductivity is roughly 100 times that of the F-region--i.e.,

$$\int_{85\ \text{km}}^{200\ \text{km}} \sigma_P\, dh \approx 10\ \text{mho}, \quad \int_{200\ \text{km}}^{500\ \text{km}} \sigma_P\, dh \approx 0.1\ \text{mho} \quad , \tag{3}$$

where

$$\sigma_P = \frac{Nq}{B}\left(\frac{\Omega_i \nu_{in}}{\Omega_i^2 + \nu_{in}^2}\right) \tag{4}$$

is the volume Pedersen conductivity. Thus, accurate simulations of these plasma processes must include field-line coupling to a conductive E layer. At present, the quantitative effects of this coupling process are not well understood; however, it is clear that significant E-region conductivity will have a damping effect on the instabilities (and the irregularities themselves) that depends on wavelength. The important questions are at what scale sizes are these effects important, and what is their wavelength dependence? The quantitative answer to these questions will require further modeling (which is currently underway at NRL) and in-situ diagnostics in conjunction with radar measurements to determine simultaneously the F-region irregularity spectrum and the E-region conductivity. It is hoped that a data set suitable for addressing these problems will be obtained as a "side benefit" of the radar support for the University of Alaska radial-shaped-charge barium release in early 1981.

In the absence of quantitative information, indirect evidence exists that indicates qualitatively that high E-region conductivity must significantly damp irregularity formation and enhance irregularity removal.

For example, if the many-hour lifetime of kilometer-scale irregularities predicted by thermal cross-field diffusion is correct (Section VII) why is there not continuous scintillation throughout the auroral zone? By the same token, there are apparently more regions of horizontal density gradient that are potentially unstable in the auroral zone than in the polar cap, which is characterized by a more uniform drizzle of precipitation. Nevertheless, scintillation levels in the polar cap generally exceed those of the auroral zone. One possible explanation for this asymmetry is the fact that the auroral zone has a more highly conducting E region than the polar cap which may play a role in removing irregularities. This interpretation is further supported by recent ac electric-field probe data from Air Force satellite OV1-17, which shows a much higher level of irregularities in the winter polar cap than in the summer polar cap (M. C. Kelley, private communication).

It is worth reemphasizing that the highly conducting auroral E layer represents a different boundary condition for model simulations of F-region instabilities from that appropriate to nighttime equatorial spread F. Thus, further detailed observations provide an opportunity to verify model predictions under varying background conditions.

VI ON THE ORIGIN AND THERMAL STRUCTURE OF AURORAL F-REGION IONIZATION ENHANCEMENTS

Several mechanisms are possible that could either produce latitudinally structured F-region plasma in the auroral zone directly or act to steepen existing horizontal plasma density gradients. Because the nighttime auroral E-region plasma is often highly structured and is produced by hard particle precipitation, perhaps the most obvious source of structured F-region plasma is soft (but still structured) electron precipitation. Once produced, the F-region ionization has a lifetime on the order of hours.

A less obvious, but possibly important source of structured F-region ionization is a spatially varying electric-field pattern. While particle precipitation is a source of plasma density enhancement, high electric fields produce density depletions. This may be seen as follows: the regions of high electric field have a higher temperature because of the enhanced Joule heating rate, q_J, given by

$$q_J = \sigma_P \left[\underline{E}_\perp + \underline{U} \times \underline{B}\right]^2 \quad , \tag{5}$$

where σ_P is the Pedersen conductivity given by Eq. (4), $\underline{E}_\perp$ is the electric field perpendicular to the geomagnetic field, $\underline{B}$, and $\underline{U}$ is the velocity of the neutral wind. One effect of an intense local enhancement in ion temperature is the change in the F-region ion composition from predominantly O^+ to NO^+. The resulting NO^+ has a higher recombination rate than O^+ and hence, a local density depletion occurs. These effects have been observed by Kelly (1979), using the Chatanika radar. Thus, a latitudinally structured electric field pattern can produce localized depletions in electron density where the magnitude of $\underline{E}$ is a maximum.

A third possible source for structured F-region plasma is a spatially varying pattern of field-aligned currents. Block and Falthammar

(1968) have shown that if field-aligned currents are carried by particles of ionospheric origin, an F-region plasma-density depletion can result. This process may act to structure F-region electron density or steepen existing structure. Data are presented below that suggest that this mechanism operates in the vicinity of E-region auroral arcs.

This set of source mechanisms for F-region blobs is not meant to be all inclusive, nor can the relative importance of each mechanism be established with the present data set. Each source mechanism listed, however, routinely occurs in the auroral ionosphere. Therefore, the fact that F-region ionization enhancements are commonplace in the auroral zone is not particularly surprising.

In addition to the ionospheric parameters described in Sections II through V, the incoherent scatter technique enables the deduction of the ionospheric electron and ion temperature. This information is useful for determining the "age" of a blob: a "young" blob is one that is being produced at the time of observation; an "old" blob is one that was produced some time ago and convected into the radar field of view. One expects a young blob to have an electron temperature, T_e, that is enhanced over the background plasma (at least if the blob were produced by precipitation); an old blob will have a T_e that is reduced at the density peak because the energy transfer rate from the electron gas is increased in regions of high electron density (Banks et al., 1974).

Figure 7, which is the same as Figure 2, shows the unstable blob discussed in detail in Section III. This blob displays the most common characteristics seen during our campaign of observations. Notice, for example, the valley between the E and F regions. Also, the bottomside of the blob is flat, which suggests that the lower portion of the blob has been evenly eroded by the height-dependent recombination rate that increases with decreasing altitude. This interpretation is supported by the thermal structure of the blob displayed in Figure 8.

The lower panel of Figure 8 shows the latitudinal variations of electron density measured at 337-km and 382-km altitude for the blob shown in Figure 7. The position of the blob is clearly seen. The two

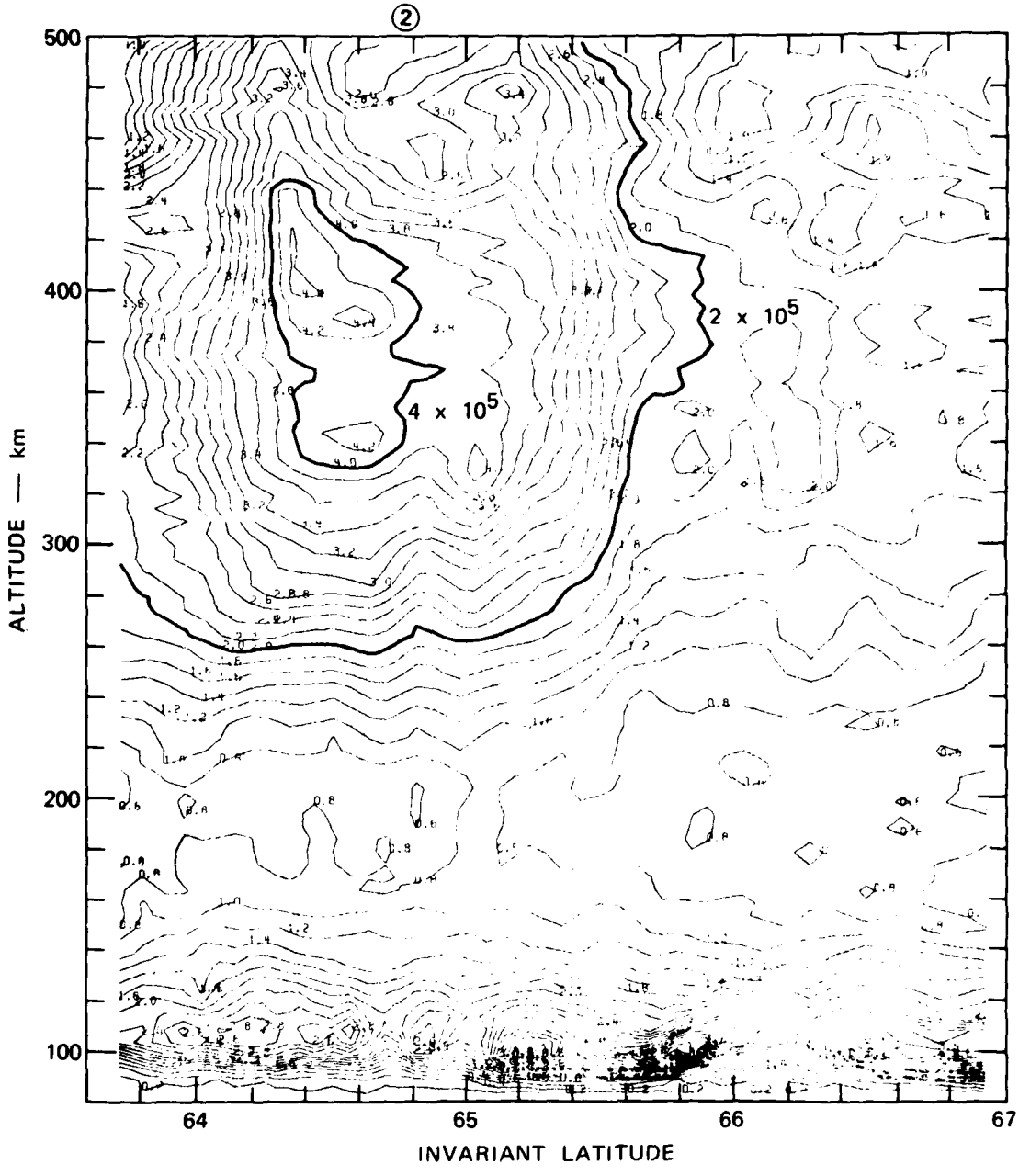

FIGURE 7 ALTITUDE/LATITUDE VARIATION OF ELECTRON DENSITY — 27 FEBRUARY 1980, 0945 TO 0958 UT

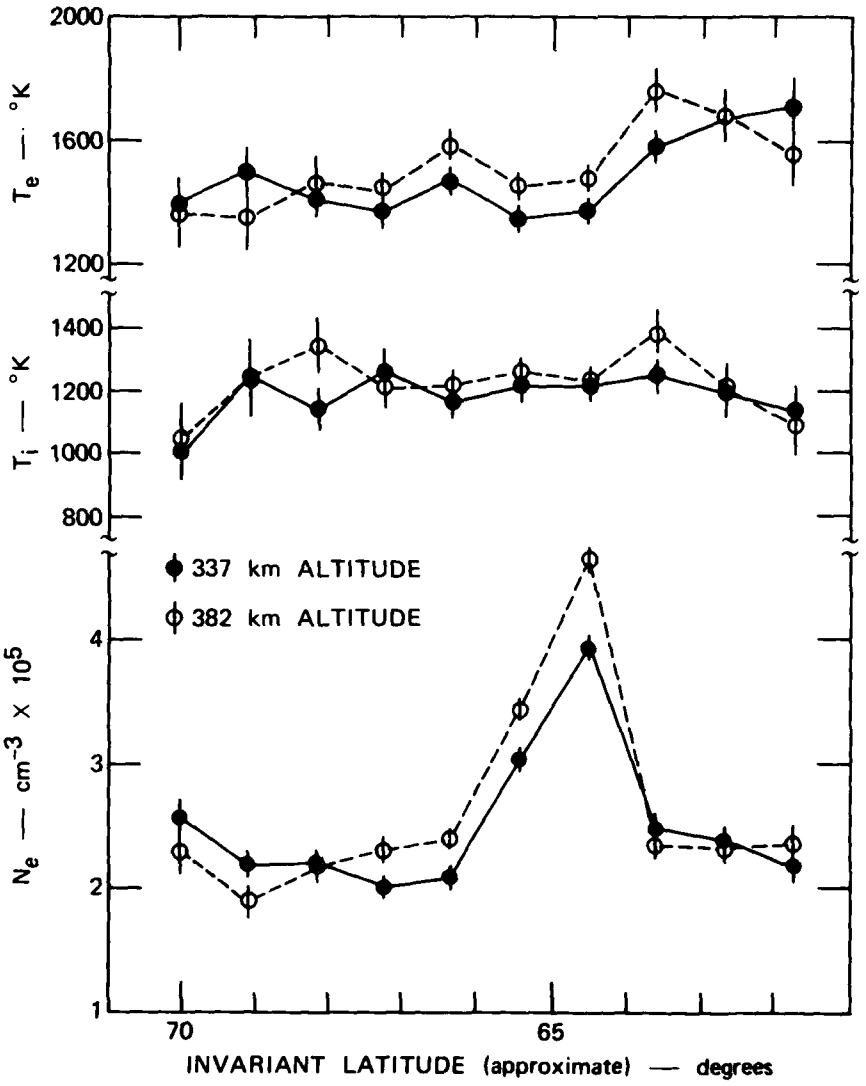

FIGURE 8 LATITUDINAL VARIATION OF ELECTRON AND ION TEMPERATURE AND ELECTRON DENSITY AT TWO FIXED ALTITUDES

upper panels show the latitudinal variations of electron and ion temperature, T_e and T_i. This example is typical in that no signature of the blob is evident in the ion temperature. Rather, the latitudinal variations in T_i reflect the variations in Joule heating with latitude.

The structure of T_e does not show the enhancement at the blob center that is expected for a young blob. On the contrary, there seems to be a slight reduction in T_e associated with the density enhancement. An even more dramatic example of this behavior is illustrated in Figure 9, which is taken from Banks et al. (1974). They kept the Chatanika radar-beam position fixed, looking northward as an F-region blob drifted south through the beam at $\sim$ 1050 UT. At the center of the blob, the electron gas is essentially in thermal equilibrium with the ion gas.

Both Figure 8 and Figure 9 show a slight increase in T_e at the blob edges, which is probably a simple consequence of the latitudinally varying energy transfer rate from the electron gas. However, the possibility of turbulent heating of electrons at the unstable edges of blobs merits further investigation.

Data from 23 February 1980 are presented in Figures 10 through 13. During the time from 1115 UT to 1205 UT, the westward electric field (southward convection) was small, and a single blob could be observed for an extended period. Figure 10 shows the altitude-latitude distribution of the electron density observed during the radar scan from 1115 UT to 1128 UT. The blob of interest is located just south of 65° invariant latitude. During this period there is a "valley" of low electron density between the E and F regions. Notice that the steepest side of the blob is the equatorward side.

Figure 11 shows data from the next radar scan taken approximately 12 min after that of Figure 10. Precipitation has filled in the valley between the E and F regions above the E-region arc. This local production of ionization distorts the bottom side of the blob in contrast to that which is observed for an old blob such as is shown in Figure 7. The steepest side of the blob is still the equatorward side although the asymmetry is not as pronounced for this scan as for the others.

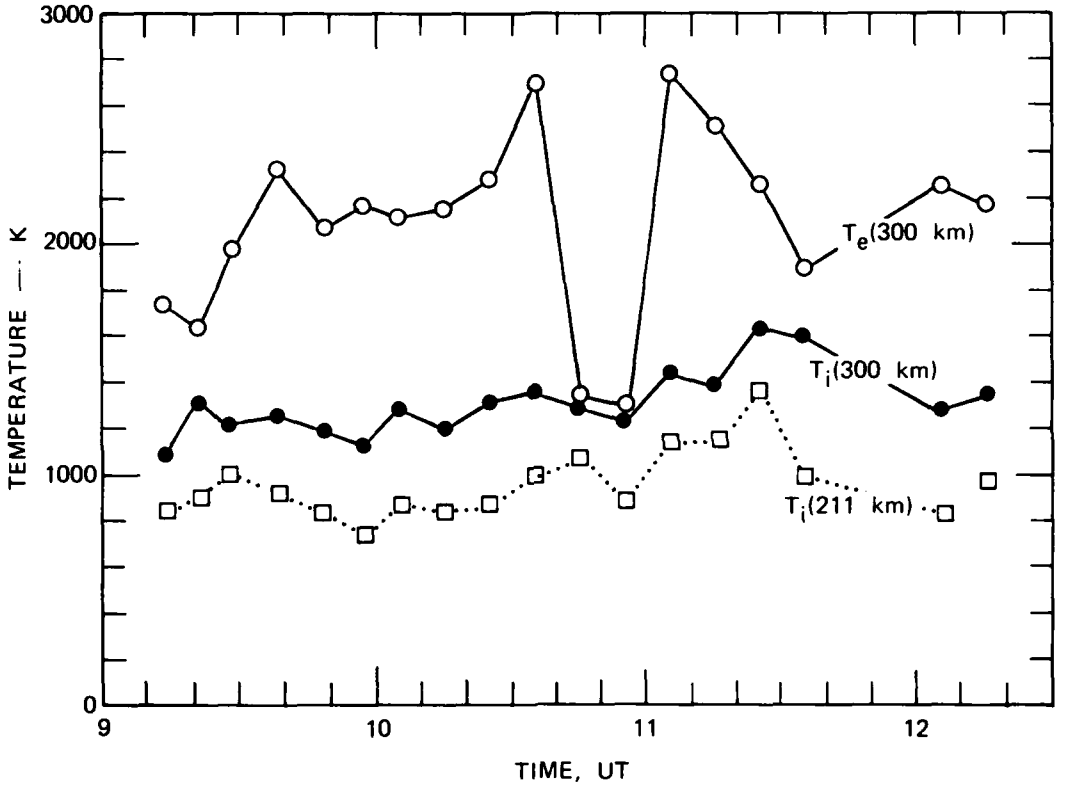

FIGURE 9 MEASURED VALUES OF ELECTRON AND ION TEMPERATURE AS AN ENHANCED F_2 LAYER PASSED THROUGH THE BEAM

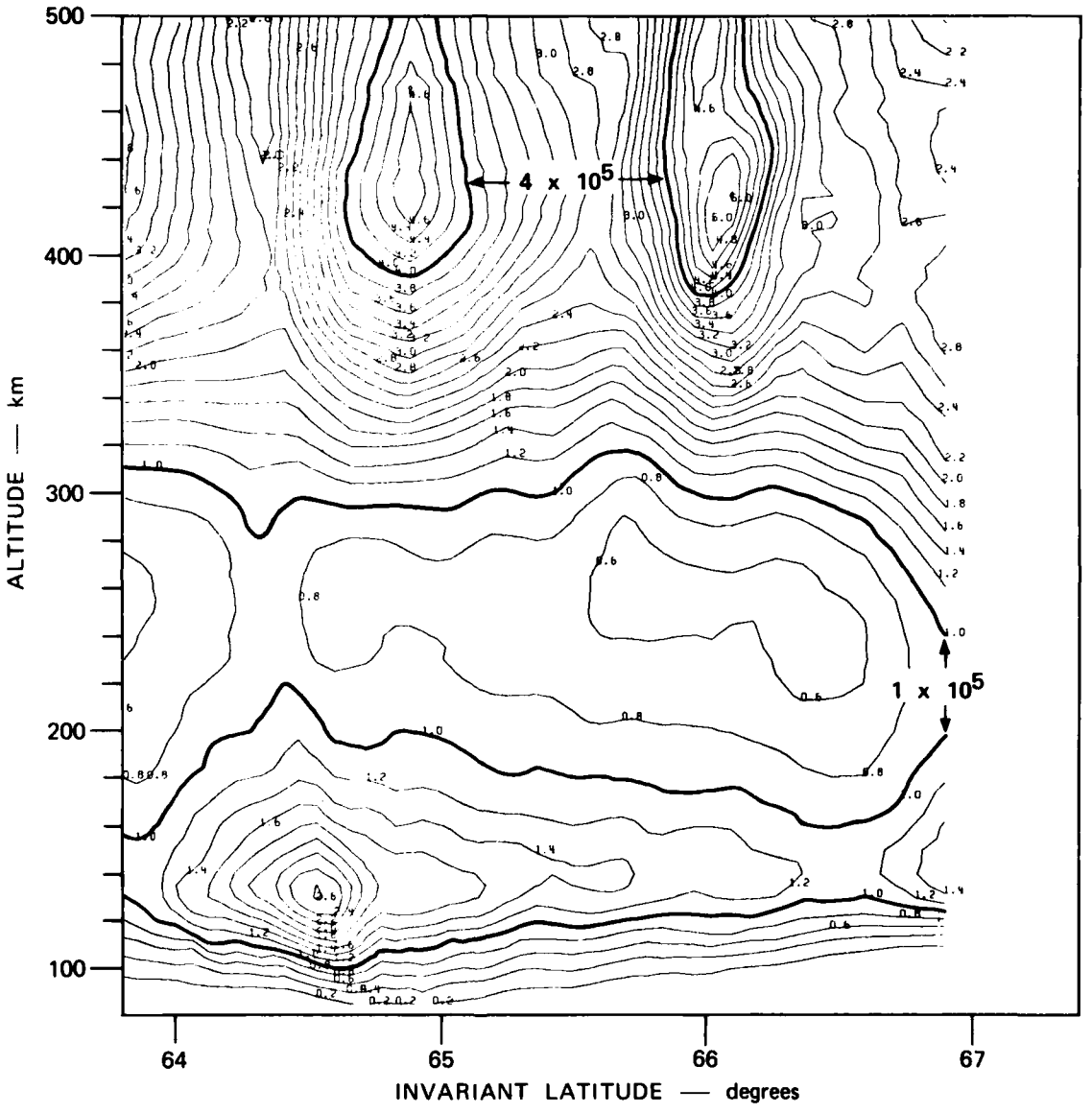

FIGURE 10 ALTITUDE/LATITUDE VARIATION OF ELECTRON DENSITY — 23 FEBRUARY 1980, 111538 TO 112810 UT

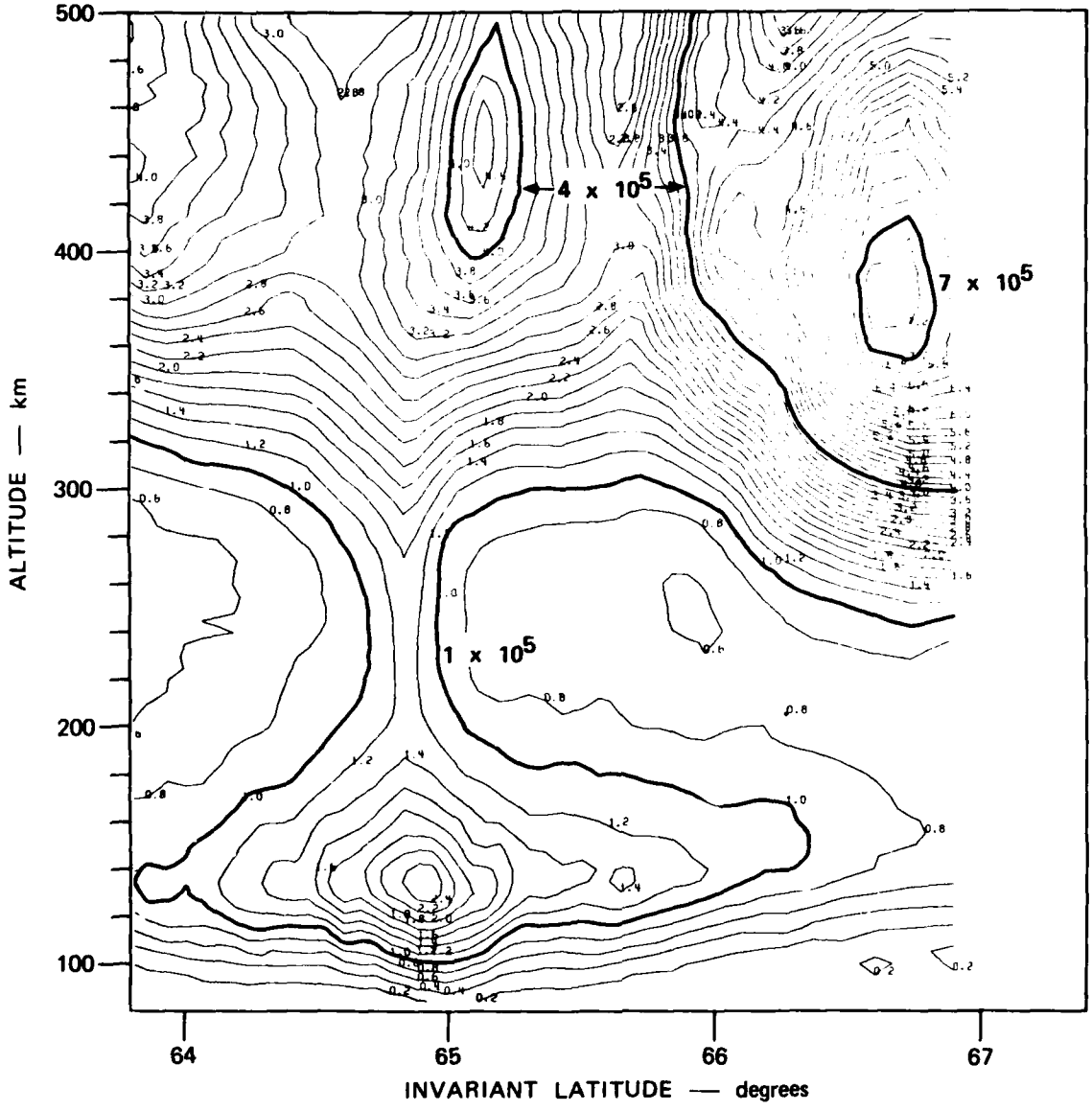

FIGURE 11 ALTITUDE/LATITUDE VARIATION OF ELECTRON DENSITY — 23 FEBRUARY 1980, 112811 TO 114043 UT

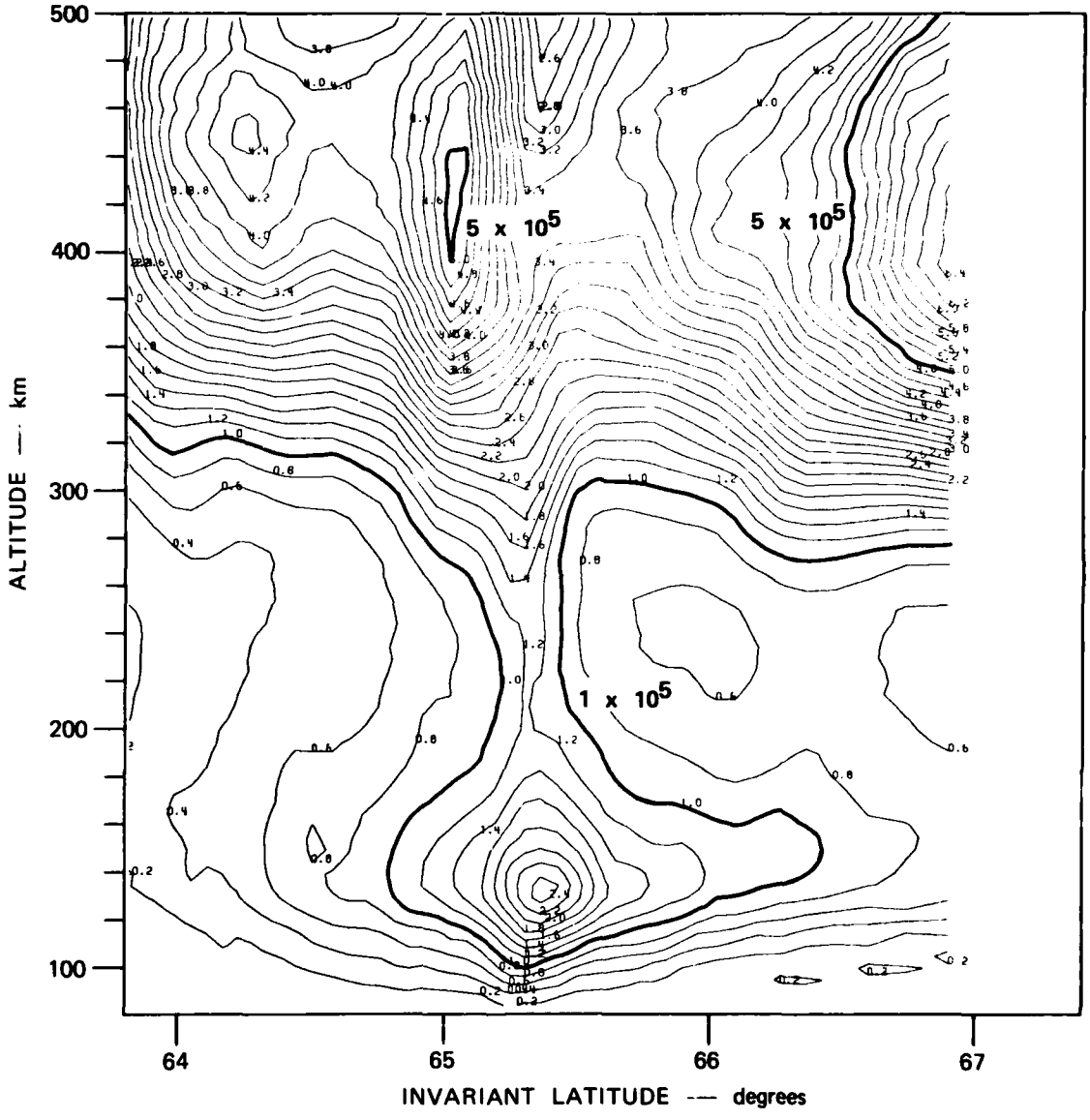

FIGURE 12 ALTITUDE/LATITUDE VARIATION OF ELECTRON DENSITY — 23 FEBRUARY 1980, 114043 TO 115316 UT

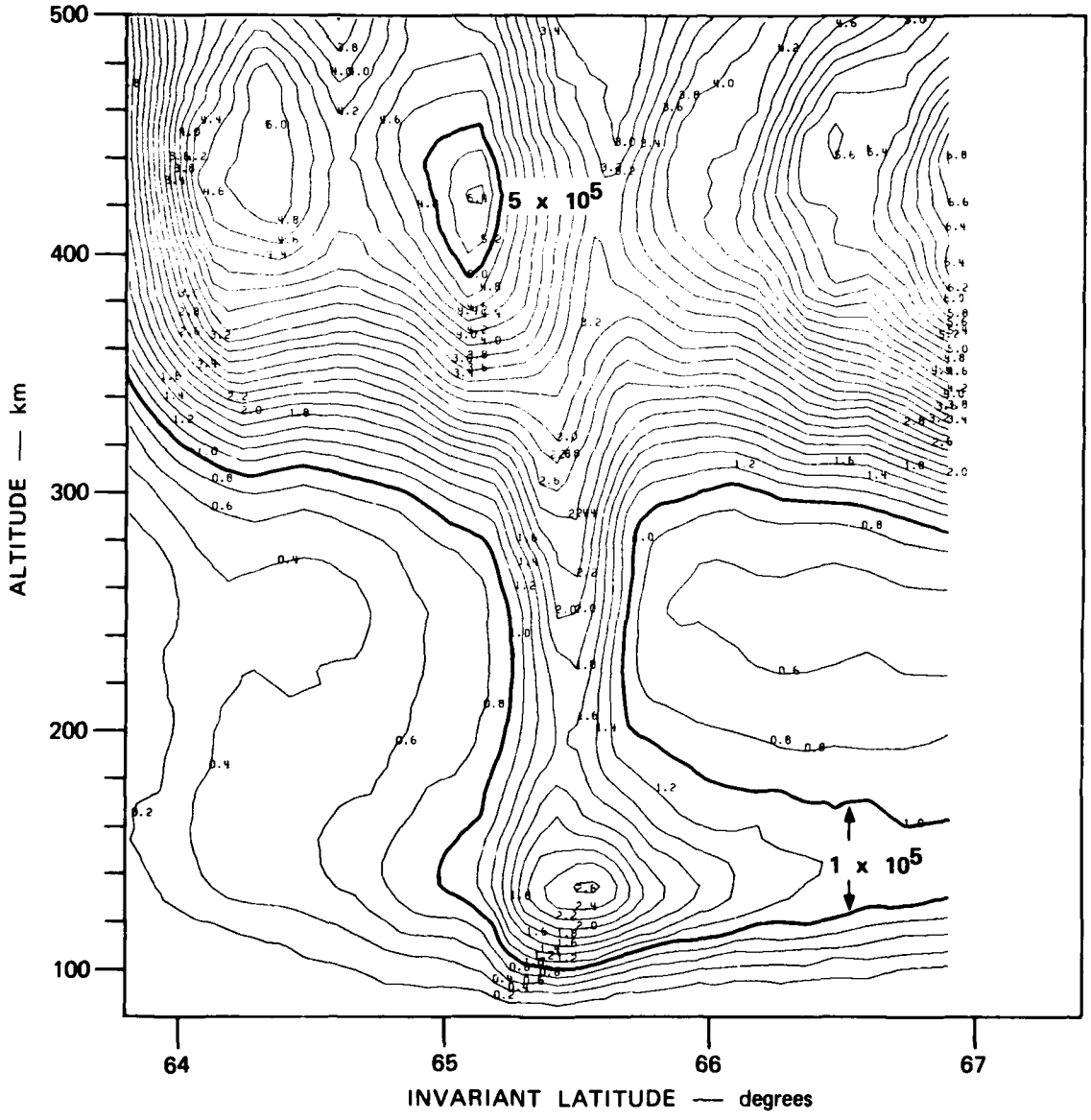

FIGURE 13 ALTITUDE/LATITUDE VARIATION OF ELECTRON DENSITY — 23 FEBRUARY 1980, 115316 TO 120549 UT

In Figure 12, data from the next consecutive scan are presented. Notice that the E-region arc has moved poleward causing the relative position of the blob with respect to the arc to change. The bottom side of the blob is now highly asymmetrical and the steepest side of the blob has changed from the equatorward side to the poleward side.

Figure 13 shows a final scan through the blob. Precipitation has filled in the E- to F-region valley over more than one half degree of latitude. Analysis of the temperatures in this region shows that T_e was enhanced by several hundred degrees throughout the "filled-in" valley. The results of this analysis support the idea that the ionization is currently being produced by precipitation; i.e., this region is "young." As in the previous scan the steepest side of the blob is the poleward side nearest the E-region arc.

As mentioned above, the zonal electric-field component was small though the period represented by Figures 10 through 13. The sign of the electric field was examined to determine which side of the blob was $\underline{E} \times \underline{B}$ unstable, and this information was correlated with which side was steepest. The steepest side of the blob was not necessarily the unstable side; however, no information is available about the direction of the neutral wind. Thus, it is possible that fluctuations in direction of the neutral wind were such that the steep side of the blob was, in fact, the unstable side. This seems unlikely, however, because in the midnight sector the neutral wind usually remains southward.

On the other hand, a one to one correlation exists between the steepest side of the blob and the one nearest the E-region arc. Therefore, it seems most likely that some aeronomical process involving the E-region arc is responsible for the edge steepening rather than a purely plasma physical process involving the stability of the edge. One such process was suggested by Block and Falthammar (1968), who showed that if field-aligned currents are carried by particles of ionospheric origin, an F-region electron-density depletion can result. Because latitudinally structured field-aligned current systems are expected in the vicinity of arcs, this is a plausible mechanism for steepening the blob

edge nearest the arc. However, there is no way to test this hypothesis with the present data set.

Another interesting aspect of the data presented in Figures 10 through 13 is the dynamic behavior of the F-region as a whole. For example, in Figure 10 a dense, narrow blob is located at 66°. However, twelve minutes later, in Figure 11, an even more dense, broad enhancement in density is centered just south of 67° invariant latitude. By the time the scan represented in Figure 12 was completed, this enhancement had moved further north. During the entire period, the blob associated with the E-region arc had not moved.

These dynamics have interesting ramifications because the ionization lifetime is so long; i.e., this apparent motion cannot be attributed to a moving source of precipitation in the magnetosphere, but must be caused by convection.

For example, if the plasma were uniform along L shells, i.e., perpendicular to the plane of this figure, then the plasma does not appear to behave as an incompressible fluid (unless one assumes unusually large and rapid changes in the height distribution of the ionization along the observed flux tubes). Therefore, it seems likely that there are zonal as well as latitudinal variations in electron density associated with blobs. These data suggest that the width of a blob may depend on longitude, and that the blob edges can have a corrugated or fluted shape. It is hoped that these questions will be answered by a proposed set of experiments designed to map both the latitudinal and longitudinal variations of F-region plasma density.

VII IRREGULARITY LIFETIME CONSIDERATIONS AND IMPLICATIONS FOR GLOBAL SCINTILLATION MORPHOLOGY

Incoherent scatter measurements have been presented from Chatanika that indicate that unstable F-region blobs are commonplace. Their presence is not simply related to magnetic activity or to E-region conditions. Measurements of the electron temperature within blobs suggest that most blobs are not locally produced by coincident soft particle precipitation. The F-region structures convect with the background electric field. Thus, in the midnight sector, the blobs are evidently produced somewhere north of Chatanika and drift southward into the radar field of view. Because the plasma density irregularities, once produced, have long lifetimes (see below), they can drift long distances from their origin.

Figure 14 shows an example of two blobs at approximately 66° and 67° invariant latitude measured near midnight on 1 March 1980. This example, unlike those presented earlier, demonstrates that blobs can exist in regions of very little E-region ionization. In this case, the blobs have drifted south of what would normally be considered the southern boundary of the diffuse auroral oval (for present purposes this boundary is defined as southernmost latitude at which the peak E-region electron-density exceeds 10^5 cm^{-3}). Thus, because of convection, the high-latitude scintillation boundary may be unrelated to any of the precipitation boundaries. In any case, to accurately predict the pattern of high latitude scintillation on a global scale, the important effects of high-latitude convection must be considered.

If the Chaturvedi-Ossakow (1979a,b) hypothesis discussed in Section II is correct, the sheet-like structure of the irregularities produced by the WIDEBAND instability indicates that the instability is saturated nonlinearly. In present theoretical treatments, the only mechanism taken into account for removing irregularities under these conditions is

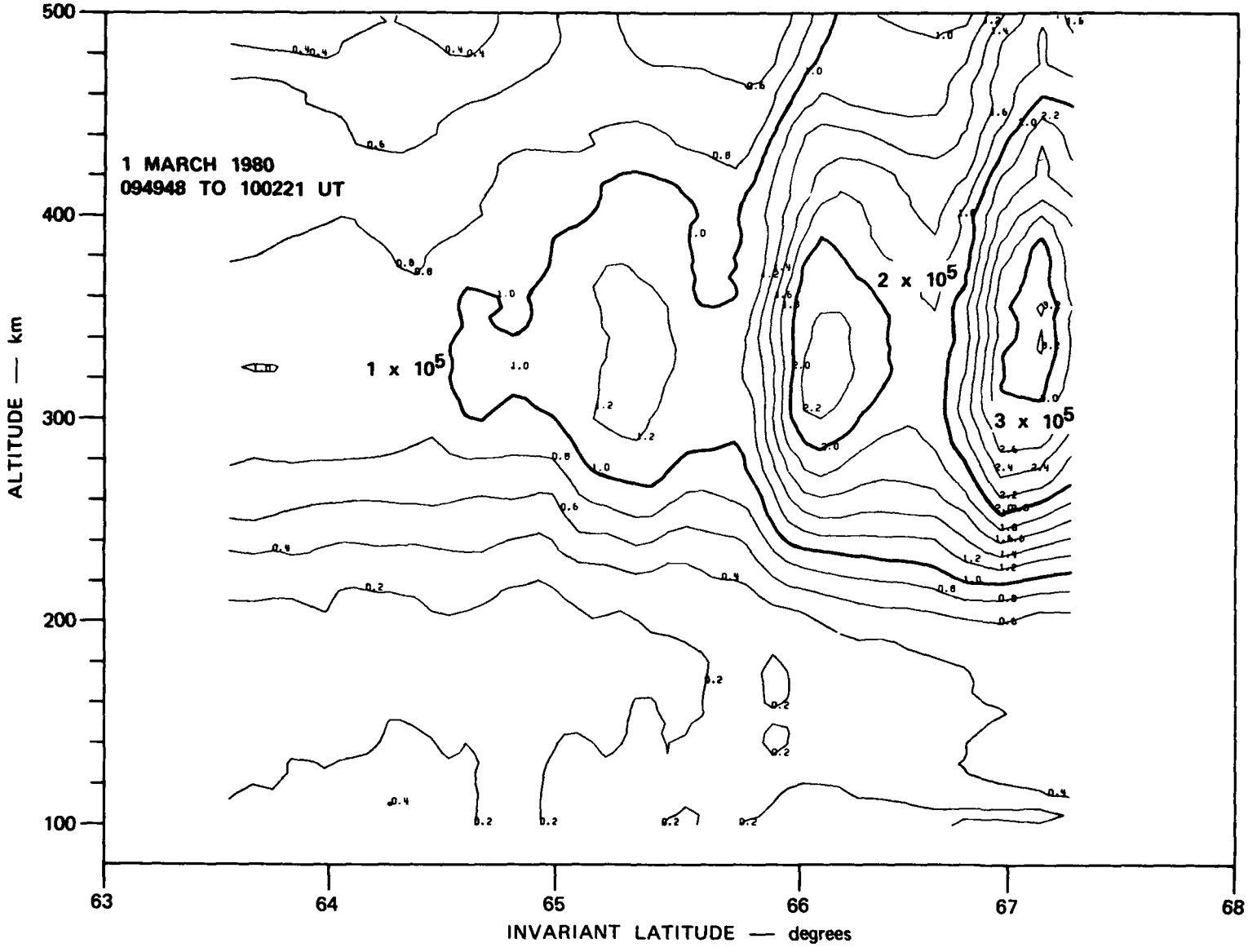

FIGURE 14 ALTITUDE/LATITUDE VARIATION OF ELECTRON DENSITY — 1 MARCH 1980, 094948 TO 100221 UT

thermal diffusion. The rate of diffusive damping (γ) of irregularities is given by:

$$\gamma = k_\perp^2 \frac{\nu_{ei}}{\Omega_e \Omega_i} C_s^2 \quad , \tag{6}$$

where $k_\perp$ is the irregularity wave number, ν_{ei} is the electron-ion collision frequency, $\Omega_{e,i}$ is the electron, ion gyrofrequency, and C_s is the acoustic speed. At F region altitudes, one can take $\nu_{ei}/\Omega_i \approx 10^{-4}$, $\Omega_i \approx 323$ Hz, and $C_s \approx 1000$ ms^{-1}. An irregularity will be reduced in amplitude by one e-fold in the time, τ, given by $\tau = 1/\gamma$. For kilometer-size irregularities, τ is approximately 23 hours. Thus, once plasma on a given flux tube becomes structured on these scale sizes, it will remain so for times that are comparable to those required to convect around the entire auroral zone.

Note that the diffusive damping rate given by Eq. (6) depends on scale size. Small scale-size irregularities diffuse away more quickly than larger ones. Thus, as a flux tube convects away from a locally unstable region, the spectrum of irregularities tied to the tube will change with time (and thus space). Because the gradient drift instability operates at essentially all wavelengths, we would expect a population of many scale sizes to be present at an unstable source region. However, at a time, τ, after the flux tube convects out of the unstable region, only irregularity wavelengths, $\lambda_\perp$, greater than a given value will survive:

$$\lambda_\perp^2 \geq (2\pi)^2 \frac{\nu_{ei}}{\Omega_e \Omega_i} C_s^2 \tau \quad . \tag{7}$$

This illustrates once again the importance of including convection effects for accurate prediction of scintillation.

It is also important to keep in mind that the scintillation levels depend critically on the ambient electron density of the ionosphere as well as its structure. The amount of time that a given flux tube spends in darkness depends on the convection pattern. In fact, some convection models predict "stagnation points" of convection where certain flux tubes

are almost never sunlit. Thus, even though F-region recombination rates are slow, the amount of scintillation should be greatly reduced in these regions. Depending on the altitude and scale size of the irregularities, the recombination rate may dominate the diffusive damping rate in determining the lifetime of irregularities that can produce significant scintillation. Also, as discussed in Section V, the presence of a highly conducting E region beneath the F-region irregularities and to which they are electrically tied via the geomagnetic field will undoubtedly limit their lifetime. A quantitative theory describing this effect is not presently available; however, such a theory is being developed. An accurate scintillation prediction model must ultimately account for all of these effects.

VIII SUMMARY

The most important results of the present research can be summarized as follows:

- Field-aligned ionization enhancements or plasma "blobs" with steep poleward and equatorward edges are a common feature of the midnight-sector auroral F region. Their presence is apparently not strongly related to magnetic activity nor to E-region processes.
- F-region plasma blobs are gradient-drift unstable on one side or the other depending on the electric field and neutral wind configuration. The presence of high-latitude field-aligned currents is a further destabilizing factor, but seldom (if ever) dominates the electric field contribution to instability.
- The presence of plasma density irregularities associated with the unstable blobs has been verified by observing scintillation of the TRIAD satellite telemetry signals at 150 MHz, which traversed the unstable region.
- The F-region irregularities exist despite the presence of a highly conducting auroral E region to which the F-region plasma is tied via the highly conducting geomagnetic field lines.
- The F-region blobs and their associated irregularities convect with the background electric field. Because large-scale ($\sim$ 1 km) irregularities can have long lifetimes (of the order of hours) they may be present far from their place of origin. As a result, there is no reason to expect a one-to-one relationship between high-latitude scintillation boundaries and precipitation boundaries.

REFERENCES

Banks, P. M., C. L. Rino, and V. B. Wickwar, "Incoherent Scatter Radar Observations of Westward Electric Fields and Plasma Densities in the Auroral Ionosphere, 1," J. Geophys. Res., Vol. 79, p. 187 ff (1974).

Banks, P. M. and G. Kockarts, Aeronomy Part A (Academic Press, Inc., New York, NY, 1973).

Block, L. P. and C.-G. Falthammar, "Effects of Field-Aligned Currents on the Structure of the Ionosphere," J. Geophys. Res., Vol. 73, p. 4807 ff (1968).

Chaturvedi, P. K. and S. L. Ossakow, "Nonlinear Stabilization of the E X B Gradient Drift Instability in Ionospheric Plasma Clouds," J. Geophys Res., Vol. 84, p. 419 ff (February 1979a).

Chaturvedi, P. K. and S. L. Ossakow, "Nonlinear Stabilization of the Current Convective Instability in the Diffuse Aurora," Geophys. Res. Letts., Vol. 6, p. 957 ff (1979b).

Fejer, B. G. and M. C. Kelley, "Ionospheric Irregularities," Accepted for publication in Rev. Geophys. and Space Phys. (1980).

Iijima, T. and T. A. Potemra, "Large-Scale Characteristics of Field-Aligned Currents Associated with Substorms," J. Geophys. Res., Vol. 83, p. 599 ff (1978).

Kelly, J. D., "Effects of Impulsive Heating Events on F-Region Chemistry and Electron Density," Topical Report, SRI Project 5915, SRI International, Menlo Park, CA, Contract DNA001-77-C-0042 (July 1979).

Ossakow, S. L. and P. K. Chaturvedi, "Current Convective Instability in the Diffuse Aurora," Geophys. Res. Letts., Vol. 6, p. 322 ff (1979).

Rino, C. L., "Power Law Phase Screen Model for Ionospheric Scintillation 1. Weak Scatter," Radio Sci., Vol. 14, p. 1135 ff (1979).

Rino, C. L., R. C. Livingston, and S. J. Matthews, "Evidence for Sheet-Like Auroral Ionospheric Irregularities," Geophys. Res. Letts., Vol. 5, p. 1039 ff (1978).

Rino, C. L. and S. J. Matthews, "On the Morphology of Auroral-Zone Radio-wave Scintillation," J. Geophys. Res., Vol. 85, p. 4139 ff (1979).

Rino, C. L. and J. Owen, "The Structure of Localized Nighttime Auroral-Zone Scintillation Enhancements," J. Geophys. Res., Vol. 85, p. 2941 ff (1980).

Rino, C. L., R. C. Livingston, B. C. Fair, and M. C. Cousins, "Continued Performance of the Wideband Satellite Experiment," Final Report, SRI Project 6434, Contract DNA001-77-C-0220, SRI International, Menlo Park, CA (March 1980).

Saflekos, N. A. and T. A. Potemra, "The Orientation of Birkeland Current Sheets in the Dayside Polar Region and its Relationship to the IMF," J. Geophys. Res., in press (1980).

Schunk, R. W. and J.C.G. Walker, "Theoretical Ion Densities in the Lower Atmosphere," Planet. Space Sci., Vol. 21, p. 1975 ff (1973).

Vondrak, R. R. and M. J. Baron, "Radar Measurements of the Latitudinal Variation of Auroral Ionization," Radio Sci., Vol. 11, p. 939 ff (1976)

DISTRIBUTION LIST

DEPARTMENT OF DEFENSE

Assistant Secretary of Defense
Comm, Cmd, Cont & Intell
ATTN: Dir of Intelligence Sys, J. Babcock

Assistant to the Secretary of Defense
Atomic Energy
ATTN: Executive Assistant

Command & Control Technical Center
ATTN: C-312, R. Mason
ATTN: C-650, G. Jones
3 cy ATTN: C-650, W. Heidig

Defense Communications Agency
ATTN: Code 480
ATTN: Code 480, F. Dieter
ATTN: Code 810, J. Barna
ATTN: Code 205
ATTN: Code 101B

Defense Communications Engineer Center
ATTN: Code R123
ATTN: Code R410, N. Jones

Defense Intelligence Agency
ATTN: DT-5
ATTN: DB-4C, E. O'Farrell
ATTN: DB, A. Wise
ATTN: DT-1B
ATTN: DIR, E. Tighe
ATTN: DC-7D, W. Wittig

Defense Nuclear Agency
ATTN: NAFD
ATTN: STNA
ATTN: RAEE
ATTN: NATD
3 cy ATTN: RAAE
4 cy ATTN: TITL

Defense Technical Information Center
12 cy ATTN: DD

Field Command
Defense Nuclear Agency
ATTN: FCPR

Field Command
Defense Nuclear Agency
Livermore Branch
ATTN: FCPRL

Interservice Nuclear Weapons School
ATTN: TTV

Joint Chiefs of Staff
ATTN: C3S
ATTN: C3S, Evaluation Office

Joint Strat Tgt Planning Staff
ATTN: JLTW-2
ATTN: JLA

Under Secretary of Defense for Rsch & Engrg
ATTN: Strategic & Space Sys (OS)

DEPARTMENT OF DEFENSE (Continued)

National Security Agency
ATTN: W-32, O. Bartlett
ATTN: B-3, F. Leonard
ATTN: R-52, J. Skillman

WWMCCS System Engineering Org
ATTN: R. Crawford

DEPARTMENT OF THE ARMY

Assistant Chief of Staff for Automation & Comm
Department of the Army
ATTN: DAAC-ZT, P. Kenny

Atmospheric Sciences Laboratory
U.S. Army Electronics R&D Command
ATTN: DELAS-EO, F. Niles

BMD Advanced Technology Center
Department of the Army
ATTN: ATC-T, M. Capps
ATTN: ATC-O, W. Davies

BMD Systems Command
Department of the Army
2 cy ATTN: BMDSC-HW

Deputy Chief of Staff for Ops & Plans
Department of the Army
ATTN: DAMO-RQC

Harry Diamond Laboratories
Department of the Army
ATTN: DELHD-I-TL, M. Weiner
ATTN: DELHD-N-P, F. Wimenitz
ATTN: DELHD-N-RB, R. Williams
ATTN: DELHD-N-P

U.S. Army Chemical School
ATTN: ATZN-CM-CS

U.S. Army Comm-Elec Engrg Instal Agency
ATTN: CCC-EMEO-PED, G. Lane
ATTN: CCC-CED-CCO, W. Neuendorf

U.S. Army Communications Command
ATTN: CC-OPS-W
ATTN: CC-OPS-WR, H. Wilson

U.S. Army Communications R&D Command
ATTN: DRDCO-COM-RY, W. Kesselman

U.S. Army Foreign Science & Tech Ctr
ATTN: DRXST-SD

U.S. Army Materiel Dev & Readiness Cmd
ATTN: DRCLDC, J. Bender

U.S. Army Missiles Intelligence Agency
ATTN: J. Gamble

U.S. Army Nuclear & Chemical Agency
ATTN: Library

DEPARTMENT OF THE ARMY (Continued)

U.S. Army Satellite Comm Agency
ATTN: Document Control

U.S. Army TRADOC Sys Analysis Actvy
ATTN: ATAA-PL
ATTN: ATAA-TDC
ATTN: ATAA-TCC, F. Payan, Jr.

DEPARTMENT OF THE NAVY

Joint Cruise Missiles Project Ofc
Department of the Navy
ATTN: JCMG-707

Naval Air Development Center
ATTN: Code 6091, M. Setz

Naval Air Systems Command
ATTN: PMA 271

Naval Electronic Systems Command
ATTN: PME 106-4, S. Kearney
ATTN: PME 117-2013, G. Burnhart
ATTN: PME 117-20
ATTN: Code 3101, T. Hughes
ATTN: Code 501A
ATTN: PME 106-13, T. Griffin
ATTN: PME 117-211, B. Kruger

Naval Intelligence Support Ctr
ATTN: NISC-50

Naval Ocean Systems Center
ATTN: Code 532, J. Bickel
ATTN: Code 5322, M. Paulson
3 cy ATTN: Code 5323, J. Ferguson
3 cy ATTN: Code 5324, W. Moler

Naval Research Laboratory
ATTN: Code 7550, J. Davis
ATTN: Code 4187
ATTN: Code 4780, S. Ossakow
ATTN: Code 7500, B. Wald
ATTN: Code 7950, J. Goodman
ATTN: Code 4700, T. Coffey

Naval Space Surveillance System
ATTN: J. Burton

Naval Surface Weapons Center
ATTN: Code F31

Naval Telecommunications Command
ATTN: Code 341

Office of Naval Research
ATTN: Code 465
ATTN: Code 420
ATTN: Code 421

Office of the Chief of Naval Operations
ATTN: OP 65
ATTN: OP 941D
ATTN: OP 981N

Strategic Systems Project Office
Department of the Navy
ATTN: NSP-2722, F. Wimberly
ATTN: NSP-2141
ATTN: NSP-43

DEPARTMENT OF THE AIR FORCE

Aerospace Defense Command
Department of the Air Force
ATTN: DC, T. Long

Air Force Geophysics Laboratory
ATTN: OPR, H. Gardiner
ATTN: OPR-1
ATTN: LKB, K. Champion
ATTN: OPR, A. Stair
ATTN: S. Basu
ATTN: PHP
ATTN: PHI, J. Buchau
ATTN: R. Thompson

Air Force Weapons Laboratory
Air Force Systems Command
ATTN: SUL
ATTN: NTYC
ATTN: NTN

Air Force Wright Aeronautical Lab
ATTN: W. Hunt
ATTN: A. Johnson

Air Logistics Command
Department of the Air Force
ATTN: OO-ALC/MM, R. Blackburn

Air University Library
Department of the Air Force
ATTN: AUL-LSE

Air Weather Service, MAC
Department of the Air Force
ATTN: DNXP, R. Babcock

Assistant Chief of Staff
Intelligence
Department of the Air Force
ATTN: INED

Assistant Chief of Staff
Studies & Analyses
Department of the Air Force
ATTN: AF/SASC, W. Keaus
ATTN: AF/SASC, C. Rightmeyer

Ballistic Missile Office
Air Force Systems Command
ATTN: ENSN, J. Allen

Deputy Chief of Staff
Operations Plans and Readiness
Department of the Air Force
ATTN: AFXOKT
ATTN: AFXOKS
ATTN: AFXOXFD
ATTN: AFXOKCD

Deputy Chief of Staff
Research, Development, & Acq
Department of the Air Force
ATTN: AFRDS
ATTN: AFRDSS
ATTN: AFRDSP

Electronic Systems Division
Department of the Air Force
ATTN: DCKC, J. Clark

DEPARTMENT OF THE AIR FORCE (Continued)

Electronic Systems Division
Department of the Air Force
ATTN: XRW, J. Deas

Electronic Systems Division
Department of the Air Force
ATTN: YSM, J. Kobelski
ATTN: YSEA

Foreign Technology Division
Air Force Systems Command
ATTN: TQTD, B. Ballard
ATTN: NIIS Library

Headquarters Space Division
Air Force Systems Command
ATTN: SKY, C. Kennedy
ATTN: SKA, D. Bolin

Headquarters Space Division
Air Force Systems Command
ATTN: YZJ, W. Mercer

Headquarters Space Division
Air Force Systems Command
ATTN: E. Butt

Rome Air Development Center
Air Force Systems Command
ATTN: OCS, V. Coyne
ATTN: TSLD

Rome Air Development Center
Air Force Systems Command
ATTN: EEP

Strategic Air Command
Department of the Air Force
ATTN: DCXT
ATTN: NRT
ATTN: DCXR, T. Jorgensen
ATTN: DCX
ATTN: XPFS

OTHER GOVERNMENT AGENCIES

Central Intelligence Agency
ATTN: OSWR/NED

Department of Commerce
National Bureau of Standards
ATTN: Sec Ofc for R. Moore

Department of Commerce
National Oceanic & Atmospheric Admin
ATTN: R. Grubb

Institute for Telecommunications Sciences
ATTN: A. Jean
ATTN: L. Berry
ATTN: W. Utlaut

U.S. Coast Guard
ATTN: G-DOE-3/TP54, B. Romine

DEPARTMENT OF ENERGY CONTRACTORS

EG&G, Inc
ATTN: J. Colvin
ATTN: D. Wright

DEPARTMENT OF ENERGY CONTRACTORS (Continued)

Lawrence Livermore National Lab
ATTN: L-389, R. Ott
ATTN: L-31, R. Hager
ATTN: Technical Info Dept Library

Los Alamos National Scientific Lab
ATTN: MS 664, J. Zinn
ATTN: D. Simons
ATTN: P. Keaton
ATTN: D. Westervelt
ATTN: E. Jones
ATTN: R. Taschek
ATTN: MS 670, J. Hopkins

Sandia National Laboratories
Livermore Laboratory
ATTN: B. Murphey
ATTN: T. Cook

Sandia National Lab
ATTN: ORG 1250, W. Brown
ATTN: ORG 4241, T. Wright
ATTN: Space Project Div
ATTN: 3141
ATTN: D. Thornbrough
ATTN: D. Dahlgren

DEPARTMENT OF DEFENSE CONTRACTORS

Aerospace Corp
ATTN: I. Garfunkel
ATTN: S. Bower
ATTN: D. Olsen
ATTN: N. Stockwell
ATTN: R. Slaughter
ATTN: V. Josephson
ATTN: T. Salmi
ATTN: J. Straus

University of Alaska
ATTN: T. Davis
ATTN: N. Brown
ATTN: Technical Library

Analytical Systems Engineering Corp
ATTN: Radio Sciences

Analytical Systems Engineering Corp
ATTN: Security

Barry Research Corporation
ATTN: J. McLaughlin

BDM Corp
ATTN: T. Neighbors
ATTN: L. Jacobs

Berkeley Research Associates, Inc
ATTN: J. Workman

BETAC
ATTN: J. Hirsch

Boeing Co
ATTN: M/S 42-33, J. Kennedy
ATTN: G. Hall
ATTN: S. Tashird

Booz-Allen & Hamilton, Inc
ATTN: B. Wilkinson

DEPARTMENT OF DEFENSE CONTRACTORS (Continued)

University of California at San Diego
ATTN: H. Booker

Charles Stark Draper Lab, Inc
ATTN: J. Gilmore
ATTN: D. Cox

Communications Satellite Corp
ATTN: D. Fang

Comsat Labs
ATTN: G. Hyde
ATTN: R. Taur

Cornell University
ATTN: M. Kelly
ATTN: D. Farley, Jr

Electrospace Systems, Inc
ATTN: H. Logston

ESL, Inc
ATTN: J. Marshall

General Electric Co
ATTN: M. Bortner
ATTN: A. Harcar

General Electric Co
ATTN: A. Steinmayer
ATTN: C. Zierdt

General Electric Co
ATTN: F. Reibert

General Electric Tech Services Co, Inc
ATTN: G. Millman

General Research Corp
ATTN: J. Ise, Jr
ATTN: J. Garbarino

Horizons Technology, Inc
ATTN: R. Kruger

HSS, Inc
ATTN: D. Hansen

IBM Corp
ATTN: F. Ricci

University of Illinois
ATTN: Security Supervisor for K. Yeh

Institute for Defense Analyses
ATTN: J. Bengston
ATTN: E. Bauer
ATTN: H. Wolfhard
ATTN: J. Aein

International Tel & Telegraph Corp
ATTN: G. Wetmore
ATTN: Technical Library

JAYCOR
ATTN: J. Sperling

JAYCOR
ATTN: J. Doncarlos

DEPARTMENT OF DEFENSE CONTRACTORS (Continued)

Johns Hopkins University
ATTN: T. Potemra
ATTN: J. Phillips
ATTN: T. Evans
ATTN: J. Newland
ATTN: P. Komiske

Kaman TEMPO
ATTN: DASIAC
ATTN: W. McNamara
ATTN: T. Stephens
ATTN: W. Knapp

Linkabit Corp
ATTN: I. Jacobs

Litton Systems, Inc
ATTN: R. Grasty

Lockheed Missiles & Space Co, Inc
ATTN: W. Imhof
ATTN: M. Walt
ATTN: R. Johnson

Lockheed Missiles & Space Co, Inc
ATTN: Dept 60-12

M.I.T. Lincoln Lab
ATTN: D. Towle

Martin Marietta Corp
ATTN: R. Heffner

McDonnell Douglas Corp
ATTN: J. Moule
ATTN: R. Halprin
ATTN: W. Olson
ATTN: G. Mroz
ATTN: N. Harris

Meteor Communications Consultants
ATTN: R. Leader

Mission Research Corp
ATTN: S. Gutsche
ATTN: R. Hendrick
ATTN: D. Sappenfield
ATTN: F. Fajen
ATTN: R. Bogusch
ATTN: R. Kilb
ATTN: Tech Library

Mitre Corp
ATTN: G. Harding
ATTN: A. Kymmel
ATTN: B. Adams
ATTN: C. Callahan

Mitre Corp
ATTN: M. Horrocks
ATTN: J. Wheeler
ATTN: W. Foster
ATTN: W. Hall

Pacific-Sierra Research Corp
ATTN: E. Field, Jr
ATTN: F. Thomas
ATTN: H. Brode

DEPARTMENT OF DEFENSE CONTRACTORS (Continued)

Pennsylvania State University
ATTN: Ionospheric Research Lab

Photometrics, Inc
ATTN: I. Kofsky

Physical Dynamics, Inc
ATTN: E. Fremouw

Physical Research, Inc
ATTN: R. Deliberis

R & D Associates
ATTN: R. Turco
ATTN: F. Gilmore
ATTN: B. Gabbard
ATTN: M. Gantsweg
ATTN: C. Greifinger
ATTN: W. Wright
ATTN: R. Lelevier
ATTN: W. Karzas
ATTN: H. Ory
ATTN: P. Haas

R & D Associates
ATTN: B. Yoon

Rand Corp
ATTN: C. Crain
ATTN: E. Bedrozian

Riverside Research Institute
ATTN: V. Trapani

Rockwell International Corp
ATTN: R. Buckner

Rockwell International Corp
ATTN: S. Quilici

Santa Fe Corp
ATTN: D. Paolucci

Science Applications, Inc
ATTN: J. Cockayne

DEPARTMENT OF DEFENSE CONTRACTORS (Continued)

Science Applications, Inc
ATTN: E. Straker
ATTN: D. Hamlin
ATTN: L. Linson
ATTN: C. Smith

SRI International
ATTN: W. Jaye
ATTN: R. Leadabrand
ATTN: D. Neilson
ATTN: C. Rino
ATTN: J. Petrickes
ATTN: W. Chesnut
ATTN: R. Livingston
ATTN: R. Tsunoda
ATTN: G. Smith
ATTN: G. Price
ATTN: M. Baron
ATTN: A. Burns
4 cy ATTN: J. Vickrey

Sylvania Systems Group
ATTN: M. Cross

Technology International Corp
ATTN: W. Boquist

TRI-COM, Inc
ATTN: D. Murray

TRW Defense & Space Sys Group
ATTN: D. Dee
ATTN: R. Plebuch

Utah State University
ATTN: L. Jensen
ATTN: K. Baker
ATTN: J. Dupnik

Visidyne, Inc
ATTN: C. Humphrey
ATTN: J. Carpenter